The Meteoritical Society

Meteoritics & Planetary Science 1–22 (2010)
doi: 10.1111/j.1945-5100.2010.01056.x

Shock and thermal history of Northwest Africa 4859, an annealed impact-melt breccia of LL chondrite parentage containing unusual igneous features and pentlandite

Niina JAMSJA and Alex RUZICKA*

Cascadia Meteorite Laboratory, Department of Geology, Portland State University, 17 Cramer Hall, 1721 SW Broadway, Portland, Oregon 97207–0751, USA
*Corresponding author. E-mail: ruzickaa@pdx.edu

(Received 29 September 2009; revision accepted 09 March 2010)

Abstract–Northwest Africa 4859 (NWA 4859) is a meteorite of LL chondrite parentage that shows unusual igneous features and contains widely distributed pentlandite. The most obvious unusual feature is a high proportion of large (≤3 cm diameter) igneous-textured enclaves (LITEs), interpreted as shock melts that were intruded into an LL chondrite host. One such LITE appears to have been produced by whole rock melting of LL chondrite, initial rapid partial crystallization, and subsequent slow cooling of the residual melt in the host to produce a differentiated object. Other unusual features include mm-sized "overgrowth objects," fine-grained plagioclase-rich bands, and coarse troilite (≤7 mm across) grains. All these features are interpreted as having crystallized from melts produced by a single transient shock event, followed by slow cooling. A subsequent shock event of moderate (S3) intensity produced veining and transformed some of the pyroxene into the clinoenstatite polytype. Pentlandite (together with associated troilite) in NWA 4859 probably formed by the breakdown of a monosulfide precursor phase at low temperature (≤230 °C) following the second shock event. NWA 4859 is interpreted to be an unusual impact-melt breccia that contains shock melt which crystallized in different forms at depth within the parent body.

INTRODUCTION

NWA 4859 is a recently discovered meteorite from Northwest Africa that shows unusual features. In broken and cut surfaces of hand specimens, both chondritic and achondritic (igneous-textured) areas are visible in a light colored interior, together with coarse sulfides and chondrule sized objects with light colored borders. To better elucidate the origin of the meteorite and its components, we studied NWA 4859 using optical petrography, scanning electron microscopy (SEM), and electron microprobe (EMPA) techniques. We infer that NWA 4959 represents a previously unrecognized type of annealed impact-melt breccia with an LL5–6 host.

METHODS AND SAMPLES

Five polished thin sections (CML 272-14A, -14B, -14C, -1, and -16) of NWA 4859 were examined using a Leica DM 2500 petrographic microscope, and three sections (CML 272-1, -14B, and -16) were studied with backscatter-electron (BSE) imaging techniques using a JEOL 35C scanning electron microscope (SEM) at Portland State University. Four thin sections (CML 272-1, -14B, -14C, -16) were analyzed using a Cameca SX-100 electron microprobe housed at Oregon State University and accessed remotely from Portland State University. Microprobe operating beam conditions were 15 kV accelerating voltage, 30 nA sample current as measured in a Faraday cup, and a beam diameter of about 1 μm. Analyses of olivine, pyroxene, feldspar, metal, and sulfide were obtained. With the analytical conditions used, minor sodium loss occurred in analyses of plagioclase feldspar. For the latter, only those analyses with a stoichiometry close to plagioclase were accepted, which satisfied the following criteria: (1) tetrahedral cations (Al + Si)/8 oxygen = 3.95–4.05, (2) alkali cations (Na + Ca + K)/8 oxygen = 0.85–1.0,

and (3) total cations/8 oxygen = 4.85–5.00 (all atomic units).

Modal data for one large object (LITE 3) were obtained with a point counting technique using BSE and reflected light micrographs, and were combined with average measured phase compositions to derive bulk compositions of different portions of the LITE. For the mode and bulk composition, area fractions were assumed to be equivalent to volume fractions, all pyroxene was assumed to be orthopyroxene, and all phosphate was assumed to be stoichiometric merrillite. For the calculation of bulk chemical composition, measured phase compositions were assumed except for merrillite, and the following mineral densities (ρ, in g cm^{-3}) from Gaines et al. (1997) were used:

$$\rho_{olivine} = 3.55, \rho_{pyroxene} = 3.38, \rho_{plagioclase} = 2.63, \rho_{kamacite} = 7.9, \rho_{taenite} = 8.14, \rho_{troilite} = 4.84, \rho_{phosphate} = 3.1.$$

Olivine grains in different thin sections of the meteorite were examined for shock deformation and were assigned a shock stage using the criteria of Stöffler et al. (1991), Schmitt and Stöffler (1995), and Schmitt (2000). Grains within the host and in different large objects (LITEs) were considered separately, with 20–45 large (> 50 microns across) grains of high interference colors studied in each object. Based on the references given above, the following criteria were used to define shock stages: S1—uniform extinction (misorientation within the grain < 2 degrees); S2—undulatory extinction (misorientation 2–3 degrees); S3—extinction as in S2 together with one to two sets of planar fractures; S4—weak mosaic extinction (multiple domains of a single grain showing 3–5 degrees misorientation), with ≥2 sets of planar fractures; S5—strong mosaic extinction (misorientation > 5 degrees, with misorientation domains tending to be smaller than for S4), together with ≥3 sets of planar fractures with or without the presence of planar deformation features; S6—recrystallized olivine. Following the recommendations of Stöffler et al. (1991), the overall shock stage was equated to the highest shock level shown by at least 25% of the grains in a particular object.

RESULTS

Overall Petrography

Optical and SEM images of NWA 4859 illustrating overall textures are shown in Fig. 1. Large portions of the meteorite display a mineralogy and texture similar to that of a type 5 ordinary chondrite, although other areas have a texture more similar to that of a type 6 chondrite (Figs. 1a and 1b). NWA 4859 also contains unusual features, most obviously a relatively high proportion of large igneous-textured enclaves (LITEs), some of which reach 3 cm in diameter (Fig. 1a; Table 1). Other unusual features include chondrule sized objects with distinct coarse-grained borders (“overgrowths”) of olivine or pyroxene (Figs. 1a and 1b; Table 1), plagioclase-rich bands that surround chondrules and LITEs, and large troilite grains that reach 7 mm across. Large (≤2 mm across) phosphate grains are also present.

Prominent rust halos are centered on the large troilite grains as well as on rare troilite rich regions. Despite the rust halos, weathering of metal is minimal, and the weathering stage is best described as W1 (Wlotzka 1993). Minor pentlandite is also found associated with troilite. Point counting of four different thin sections (10,000 points each) indicates that the modal abundance of metal and sulfides in NWA 4859 is 1.3 vol% and 4.5 vol%, respectively, which is consistent with the average metal and sulfide bulk composition of LL chondrites (Jarosewich 1990; Reed and Chinner 1995).

NWA 4859 was clearly affected by shock deformation and melting. The most obvious manifestation of shock melting is opaque shock veins. These are usually troilite rich, vary in width from a few to 250 microns, and reach up to approximately 1 cm in length (Figs. 1a, 1c, and 1d). Silicate clasts consisting of olivine and pyroxene, and never plagioclase, are sometimes found embedded in these veins (Fig. 1c). The proportion of troilite and silicate in the veins varies, with some areas containing massive troilite with little silicate, to areas containing troilite between silicate clasts, to areas containing droplets of troilite within a cryptocrystalline silicate groundmass. No glass was observed in the veins. Opaque shock veins crosscut the host as well as all other objects. They often occur at the boundaries between LITEs and the host (Fig. 1a; Table 1). In places, large troilite grains are clearly displaced along intersecting veins.

NWA 4859 shows other evidence for shock metamorphism. This includes planar fractures and undulatory or mosaic extinction in olivine (Stöffler et al. 1991), polycrystalline troilite grains (Bennett and McSween 1996), and chondrules whose shapes appear to have been distorted by plastic deformation. In addition, NWA 4859 contains potential shock indicators, including a relatively high proportion of chromite-plagioclase intergrowths (e.g., Rubin 2003), as well as a small amount of twinned low Ca pyroxene of the clinoenstatite polytype (e.g., Rubin 2002). However, all plagioclase in NWA 4859 appears to be crystalline and no shock produced maskelynite was found.

Different intensities of shock deformation are observed for olivine in different areas (Fig. 2). Grains

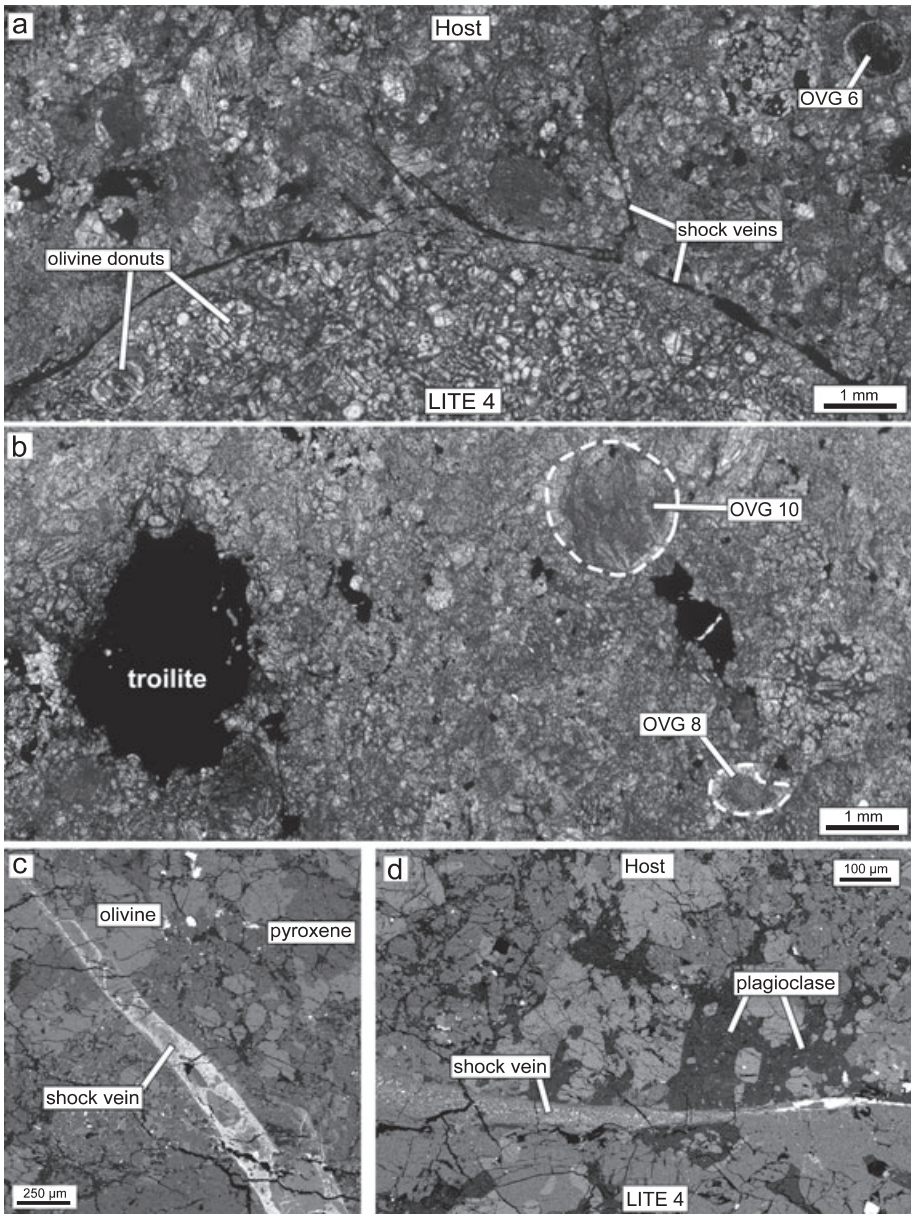

Fig. 1. Images showing large-scale features in NWA 4859. a) Thin section scanner micrograph in transmitted light showing a type 5-like texture of the host chondrite, and an adjacent portion of LITE 4. Opaque shock veins encircle the LITE and branch out into the host and crosscut the LITE. Grains of olivine, the predominant phase visible LITE 4, are often observed in shapes that resemble donuts. OVG 6 is located in upper right corner of the micrograph. b) Thin section scanner image in transmitted light showing a type 6-like texture. Two OVG objects (OVG 8 and 10) are visible, as well as coarse troilite. c) A BSE image of a portion of a troilite-rich shock vein that contains silicate clasts. This vein, reaching at least 9 cm in length, is one of the largest shock veins in NWA 4859. d) BSE image of an opaque shock vein at the contact between LITE 4 and the host, which varies in thickness from approximately 10 to 100 microns and which, like other veins, crosscuts plagioclase-rich regions.

within each of the areas show a range of shock characteristics, which is to be expected as a result of the heterogeneous shock effects that can be produced when a shock wave passes through chondritic materials (e.g., Sharp and DeCarli 2006). However, all LITEs except possibly LITE 1 contain olivine grains that show less deformation on average than in the host. The host is best described as shock stage S4; LITEs 7 and 8 are best described as shock stage S3; and whereas LITEs 4 and 9 can be described as shock stage S4, they have a larger proportion of weakly deformed olivine grains than the host (Fig. 2). There is no correlation between the intensity of olivine deformation and the overall mineralogy, texture, or location of the areas.

Table 1. Petrographic data for distinctive objects in NWA 4859.

Object[1]	Size[2] (mm)	Interior texture[3]	Edge features[3]
LITE 1	>17	Ol microporphyry	Ol rich interior border; partial shock vein and plag bands
LITE 2	3 × 3.5	Coarse px	Partial plag band, indistinct edge
LITE 3	3.5 × 4.5	(a) Skeletal, ol rich (b) coarse granular, ol poor	Indistinct edge in places
LITE 4	15 × 17[4]	Ol microporphyry, with ol "donuts"	Complete shock vein, partial plag bands
LITE 5	>8.5	Core skeletal ol, radiating; outer poikilitic	Partial shock vein, indistinct edge
LITE 6	>5	Core barred ol–px; outer granular	Indistinct edge
LITE 7	1.9 × 3.6	Ol microporphyry	Ol rich interior border
LITE 8	>26	Ol microporphyry	Partial shock vein and plag bands
LITE 9	4.6	Skeletal/barred ol	Indistinct edge
OVG 1	1.7	Fine px	Coarse px, accessory met, troi (40–130 μm thick shell)
OVG 2	1.9	Fine px	Coarse px, accessory met, troi (100–260 μm thick shell)
OVG 3	0.8	Elongate ol, plag–chr mesostasis	Coarse ol, accessory met, troi, chr (100–200 μm thick shell)
OVG 4	0.8 × 1.2	Px rich, troi + plag	Coarse px (60–280 μm thick shell)
OVG 5	2	Granular ol	Coarse px, accessory troi, met, chr (150–450 μm thick shell)
OVG 6	0.9	Ol bars, plag + chr mesostasis	Coarse ol (40–130 μm thick shell); complete plag band
OVG 7	1.7	Px rich, fine to radiating	Coarse ol (50–150 μm thick shell); plag band
OVG 8	1.3	Px rich, troi + plag + met	Coarse px (220–350 μm thick shell)
OVG 9	1.7	Equant-tabular ol–px	Coarse px, troi at inner edge (60–180 μm thick shell)
OVG 10	1.7	Px rich	Coarse px (70 μm thick shell)
OVG 11	1.7 × 2.1	Barred px	Coarse px (100–215 μm thick shell)

[1]LITE, large, igneous-textured enclave; OVG, object containing coarse-grained border and finer grained interior.
[2]Apparent diameter in thin section.
[3]Ol, olivine; px, low Ca pyroxene (mainly orthopyroxene); plag, plagioclase; chr, chromite; met, metal; troi, troilite.
[4]Observed also in successive slab cuts, where the object was measured with a maximum diameter of 26 mm × >30 mm in orthogonal directions.

Plagioclase-rich Bands

Plagioclase in NWA 4859 commonly appears as plagioclase-rich bands 60 to 400 microns wide and up to several mm long. The bands are obvious in BSE images (Fig. 3). They consist of fine-grained (typically <30 μm across) plagioclase interstitial to granular olivine or (less commonly) pyroxene. The bands typically lack the fine-grained metal or troilite droplets associated with opaque shock veins. They have indistinct edges, locally grade into the host, and fill spaces around and between chondrules or other objects (Figs. 3a and 3b). Olivine and pyroxene grains within plagioclase bands typically have rounded edges, and sometimes show euhedral-subhedral textures, although some grains have more angular edges and could be clasts (Fig. 3c).

Plagioclase-rich bands commonly occur at the edges of chondrules, chondrule-like objects, and LITEs. However, such bands are absent around coarse (>1 mm across) sulfide grains. At the edges of LITEs, the bands occur either with or without a nearly coincident opaque shock vein that crosscuts the plagioclase (Fig. 1d). Although many instances of shock veins crosscutting plagioclase bands were found, no clear evidence was found for the reverse.

Several other regions of plagioclase concentration are present in NWA 4859. These plagioclase-rich areas are up to 400–600 μm in diameter and have circular or elongate configurations. Within these areas, plagioclase is intergrown with chromite, olivine, and pyroxene (Fig. 3d), and sometimes grains of troilite and metal. Good examples of angular, apparently clastic, olivine and pyroxene grains that are possibly flow-aligned have been observed in some plagioclase-chromite areas (Fig. 3d). These areas grade into plagioclase-rich bands that lack chromite and which contain more rounded olivine (Fig. 3e).

Large Igneous-Textured Enclaves (LITEs)

In NWA 4859, large igneous-textured enclaves (LITEs) have various igneous textures, range in size from 4 mm to 3.0 cm across, and occupy approximately 30% of all five thin sections studied in this meteorite. Table 1 summarizes petrographic data for the nine LITEs that were observed. These objects are typically poor in metal and troilite, and rich in olivine. Large, igneous-textured objects in chondrites previously have been described as "megachondrules" or "large, igneous-textured clasts" (e.g., Binns 1967; Bridges and Hutchison 1997; Ruzicka et al. 1998, 2000). However,

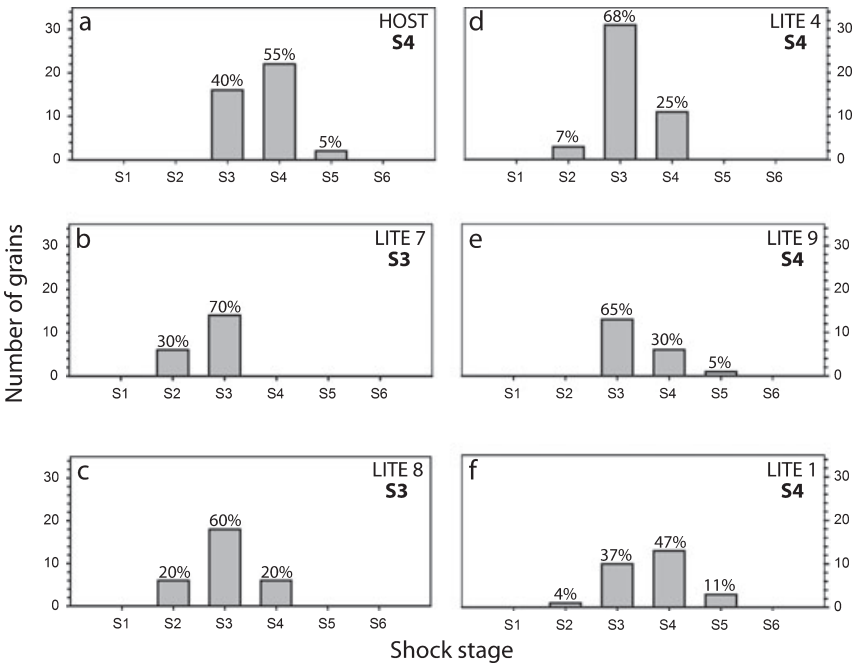

Fig. 2. Shock classification of the host (including all non-LITE areas) and several LITEs showing the number of analyzed grains and the percentages associated with each of the shock stages. Data for LITE 4 and the host are based on observations of multiple thin sections.

we prefer the more neutral term "enclave" here as it avoids the connotation of the objects being either chondrules or clasts. NWA 4859 contains other objects resembling igneous enclaves, but which are smaller than 4 mm in diameter. The LITEs can be grouped into five textural types that are described below.

Olivine Microporphyries (LITEs 1, 7, and 8)

LITEs 1, 7, and 8 are olivine microporphyries that have textures reminiscent of those in many microporphyitic olivine chondrules (Gooding and Keil 1981; Nagahara 1983; Hewins and Radomsky 1990; Hewins 1997; Hutchison 2004) (Fig. 4). These objects contain olivine phenocrysts up to 1.5 mm across set in a holocrystalline groundmass composed mainly of pyroxene and plagioclase. Larger olivine grains often have euhedral outlines, with or without embayed margins and "hollow" interiors. These LITEs are metal poor and troilite poor, containing a dozen or less micron sized opaque grains.

The borders of these LITEs vary in appearance and mineralogy (Table 1). For instance, the boundary between LITE 1 and the host has a discontinuous plagioclase-rich band that in places is cut by a thin (5–15 μm) opaque shock vein (Figs. 3e and 4). Inside of its outer edge, LITE 1 has an inner border composed of an almost continuous, 100–200 μm wide band of coarse olivine phenocrysts (visible as a light band in Fig. 4). The boundary of LITE 8 is marked by multiple shock veins and has a convoluted appearance. Some shock veins follow the LITE boundary while others clearly crosscut the LITE and displace its boundary. In other areas, a discontinuous outer plagioclase band as well as an inner olivine- and pyroxene-rich (plagioclase-poor) band mark the LITE-host boundary. Where not bounded by an opaque shock vein, the edge of LITE 8 is difficult to discern as it appears similar to the surrounding host. The edge of LITE 7 is also difficult to identify for the same reason.

Barred or Skeletal Objects (LITEs 5, 6, and 9)

LITEs 5, 6, and 9 are best described as having an overall barred or skeletal olivine texture throughout much of their interiors, with locally parallel arrangements of olivine grains that range greatly in width between the objects.

LITEs 5 and 6 are both dominated by skeletal olivine textures. Within both objects, olivine grains are locally arranged in different domains characterized by different bar and crystallographic orientations (Fig. 5a). In LITE 6, olivine bars toward the edge of the object are aligned parallel to the edge, whereas in LITE 5, the bars have a tendency to form a more radiating pattern from one edge of the object. Areas between olivine bars

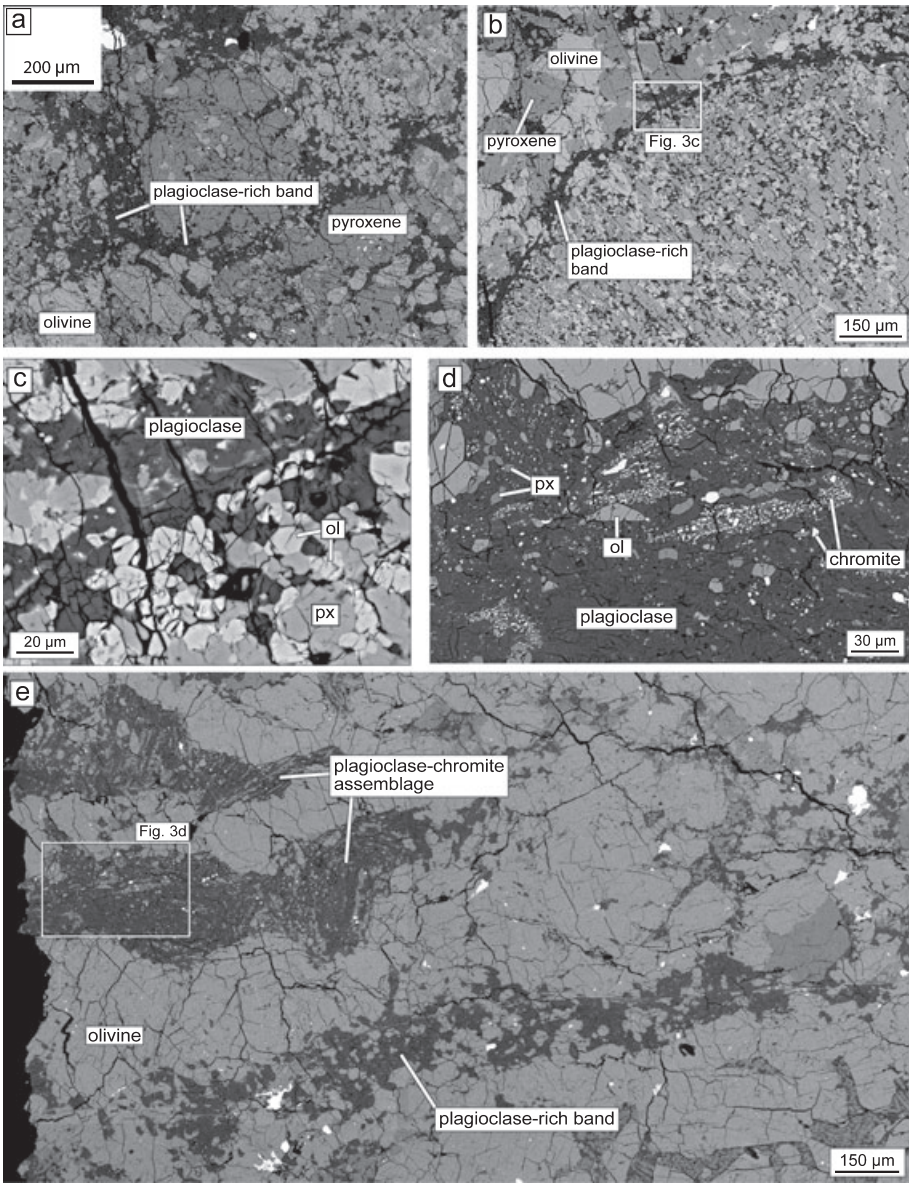

Fig. 3. BSE micrographs of plagioclase-rich regions. a) Extensive development of plagioclase-rich bands around a polycrystalline orthopyroxene-rich assemblage in the center of the image. b) A plagioclase-rich band encircles a round chondrule-sized object composed of fine-grained pyroxene, olivine, and plagioclase. c) Close-up of plagioclase band from part b, showing plagioclase filling the interstices of olivine and pyroxene grains, most of which have rounded, apparently euhedral-subhedral outlines (e.g., ol, px). Other olivine grains (e.g., at upper right) have more angular margins. d) Close-up of an elongate plagioclase-rich region containing chromite grains, as well as angular olivine (ol) and pyroxene (px) grains that are probably clasts. e) Image illustrating the different appearance of plagioclase-chromite assemblages and plagioclase bands. The prominent, labeled plagioclase band separates LITE 1 (below) from the host (above). Near the center, a smaller plagioclase band grades into a plagioclase–chromite assemblage.

in both objects are composed of coarser pyroxene and a mesostasis of plagioclase and micron sized chromite. One unusually coarse phosphate grain also occurs in the interior of LITE 5 (Fig. 5a). Low-Ca pyroxene within a given domain sometimes has a single crystallographic orientation. Olivine bars in LITE 5 are much thinner (5–15 µm) and more acicular than in LITE 6 where olivine bars are roughly 40–60 µm thick. The textures of LITEs 5 and 6 change toward their boundaries with the host, with olivine grains becoming less acicular and more equant, the olivine/pyroxene proportion decreasing, and the texture changing from barred-acicular to more poikilitic (pyroxene enclosing olivine). LITEs 5 and 6 both have incomplete shock veins

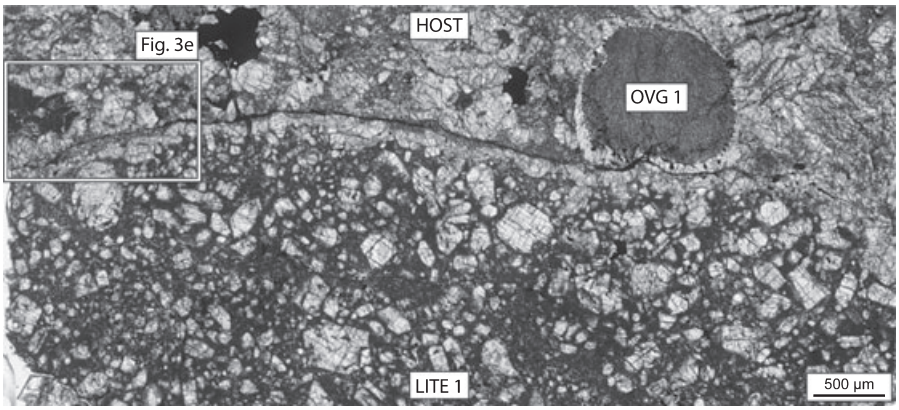

Fig. 4. Thin section scanner micrograph in transmitted light showing a portion of olivine microporphyry LITE 1. An opaque shock vein and inner olivine border (light band) is visible along much of the LITE edge. OVG 1 occurs at the edge of the LITE.

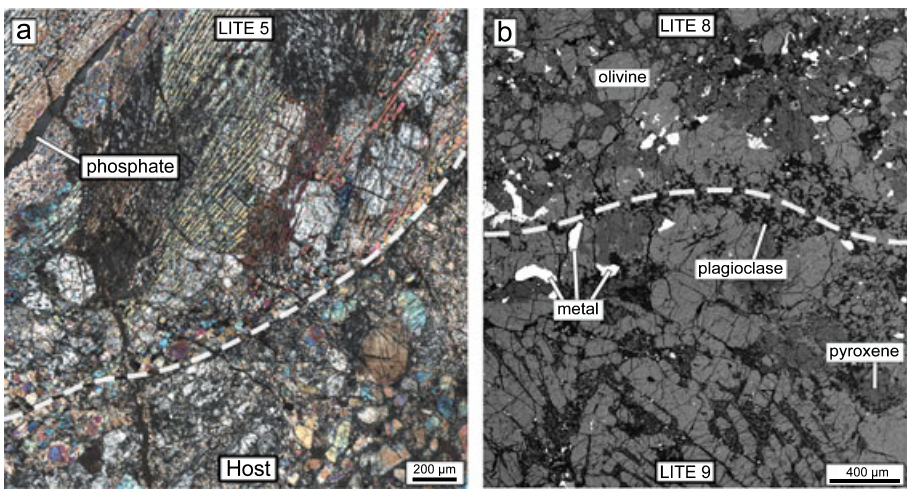

Fig. 5. Images of barred/skeletal LITEs. a) Cross polarized light image of LITE 5 showing a gradational contact with the host (dashed lines), and interior domains composed of locally parallel olivine bars and intervening low Ca pyroxene. Within each domain, olivine and pyroxene tend to have a fixed crystallographic orientation. The texture of the LITE becomes more granular and poikilitic toward the edge of the object. b) BSE micrograph shows a portion of LITE 9, which has a barred olivine core that changes to a more poikilitic texture to the edge, and the edge of LITE 8, which is an olivine microporphyry that becomes more pyroxene-rich and less porphyritic at the edge. The two enclaves are separated by a plagioclase-rich band, which is outlined by a white dashed line.

associated with their borders. Where these veins are absent, the edges of the objects appear to merge into the host (Fig. 5a).

LITE 9 contains coarser olivine bars varying from 60–130 μm in thickness and a groundmass of pyroxene and plagioclase (Fig. 5b). All of the olivine grains in the core region have parallel extinction and are aligned in the same direction. Several small grains of phosphate are present in the inner portion of this object. The texture of LITE 9 changes toward its edge, showing fewer olivine bars, more equant but still elongate olivine grains oriented in different directions, and a higher pyroxene/olivine proportion toward the host (Fig. 5b). The edge of the object is difficult to discern, except where the object appears truncated by an opaque shock vein. Where not truncated, a plagioclase band marks what could be the outer edge of LITE 9 (Fig. 5b).

Pyroxene-rich Object (LITE 2)

LITE 2 (Fig. 6) is the only enclave that is primarily composed of pyroxene. The object consists largely of relatively coarse, polycrystalline orthopyroxene (about 0.1–0.5 mm across) although some pyroxene is twinned and consists of the clinoenstatite polytype. Olivine, plagioclase, and an oxide mineral are accessory phases. The edge of the object is indistinct, although the boundary in places is marked by a plagioclase-rich band.

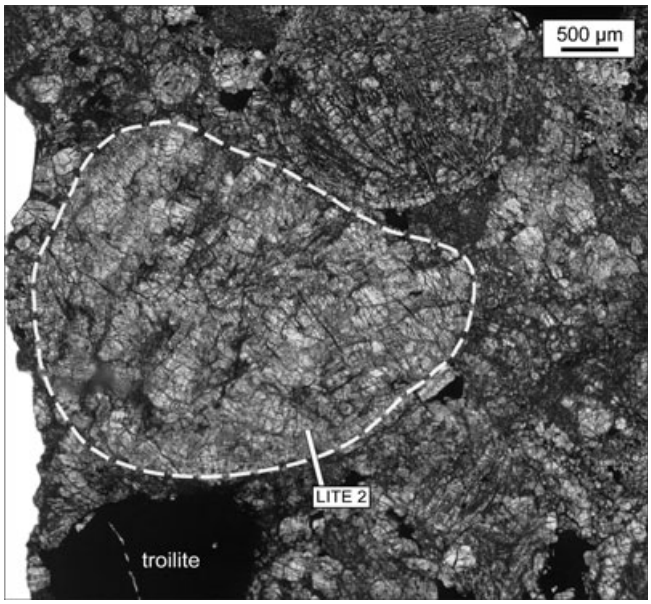

Fig. 6. Thin section scanner image in transmitted light showing LITE 2, a coarse pyroxene-rich object. A circular chondrule-like object at upper right has a barred/acicular texture similar to LITE 5, but is a smaller object.

Olivine Microporphyry with "Donuts" (LITE 4)

LITE 4 is a variant of olivine microporphyry in which olivine grains often form shells or "donuts" ranging from 0.2 to 1 mm in diameter (Figs. 1a and 7). Olivine in each donut shell has a single crystallographic orientation and thus appears to be a single grain. The donuts sometimes form a texture reminiscent to that of barred olivine chondrules, with elongate bars of olivine extending across the donuts (Fig. 7b). The mesostasis of LITE 4 between and within donuts is similar and is composed of fine-grained plagioclase, olivine and pyroxene, as well as coarser pyroxene that fills the remaining spaces between coarser olivine grains (Fig. 7). Plagioclase in the mesostasis of LITE 4 tends to form bands intergrown with fine-grained olivine adjacent to coarser olivine grains, with a texture reminiscent to that of plagioclase-rich bands in the host of the meteorite except on a smaller scale (Fig. 7b). Donuts in NWA 4859 are almost exclusively limited to LITE 4, although we did observe two isolated donuts as apparently independent objects in the host outside of LITE 8. LITE 4 has a well defined and complete opaque shock vein border that is composed of metal, troilite, and cryptocrystalline silicates (Fig. 1a). This shock vein varies in thickness from 10–180 μm and is often embedded within a plagioclase-rich band. Other shock veins crosscut the LITE. In places, LITE 4 has an inner border that is rich in pyroxene and poor in mesostasis.

Dichotomous Object (LITE 3)

LITE 3 has a dichotomous texture, with approximately 44% of the object rich in relatively coarse (> 50–100 μm) orthopyroxene and plagioclase, and approximately 56% consisting primarily of fine-grained (≤6 μm) olivine (Fig. 8). The fine-grained portion partially envelopes the coarse part of the object, with coarse troilite and metal tending to occur at the contact of the two regions but located mainly in the coarse portion (Fig. 8).

The olivine-rich portion of LITE 3 is composed primarily of thin skeletal olivine grains (4–6 μm wide) aligned in different (often perpendicular) orientations to form a tweed or cross-hatched texture. Fine-grained pyroxene, plagioclase, and a small amount of metal and subequal troilite are also present. This portion of the object has a well defined edge against the host, marked by a sharp change in mineralogy and texture.

The coarser portion of LITE 3 contains low-Ca pyroxene, plagioclase (which is sometimes twinned), and phosphate (Fig. 8b). Pyroxene often poikilitically encloses plagioclase grains, and olivine occurs both as skeletal grains close to the fine-grained portion of the object as well as intergrown coarse grains. In addition, coarse grains of troilite and subequal metal, a minor amount of mesostasis composed of high-Ca pyroxene and plagioclase, and a minor amount of chromite occur in the coarse portion of the LITE. In places where the fine-grained olivine portion is absent, the contact between the coarse portion of the LITE and the host is indistinct.

Table 2 shows the modal and bulk composition of LITE 3. The overall bulk composition of LITE 3 is similar to an average LL chondrite. CaO appears to be depleted in bulk LITE 3 compared with LL chondrite, but this is partly an artifact of counting all pyroxene in the object as orthopyroxene, ignoring the high-Ca pyroxene present in the LITE. The coarse portion of the enclave is very different and has a composition similar to that of an LL chondrite in which approximately 70% of the olivine has been removed, with this comparison most clearly made on a metal-free and sulfide-free basis (see third and sixth data columns in Table 2). LITE 3 is relatively rich in metal and troilite (Table 2), unlike other enclaves that contain only accessory metal and troilite.

Overgrowth Objects (OVGs)

NWA 4859 contains chondrule-sized objects that are surrounded by distinctive coarse-grained borders that differ from typical textures reported for chondrules. These objects are visible in hand specimen as well as in thin sections and are here called overgrowth objects (or

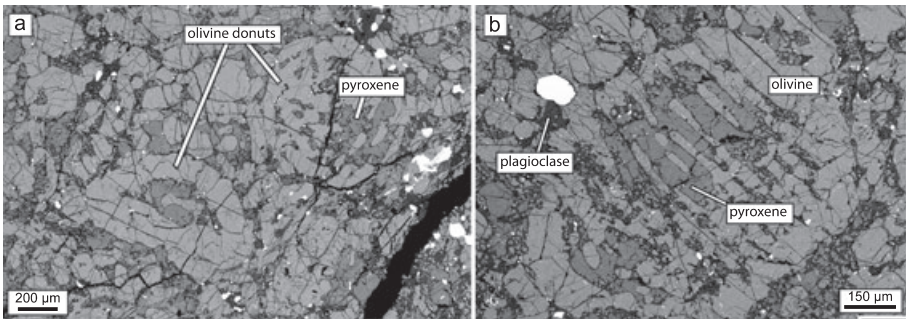

Fig. 7. BSE micrographs of LITE 4, an olivine microporphyry that contains ''donut-shaped'' olivine. a) Details of two olivine donuts among surrounding material. Accessory opaques (white) of LITE 4 are visible on the right side of the image. b) A well defined example of an olivine donut with a barred olivine texture. Orthopyroxene and plagioclase occur between olivine grains, with most plagioclase ''wetting'' olivine grains in a texture reminiscent of plagioclase bands in the host.

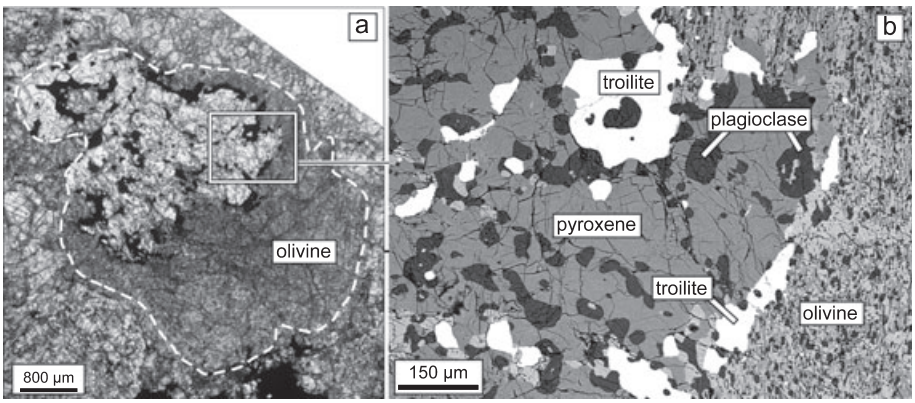

Fig. 8. Images of dichotomous object LITE 3. a) Outlined LITE 3, as it appears in transmitted light with a thin section scanner, contains an inner, coarser-grained region that is partly surrounded by a region of finer-grained polycrystalline olivine. Individual bars in the olivine-rich portion are only approximately 5 μm thick, too small to resolve in this image. b) Close-up BSE micrograph shows the occurrence of relatively equigranular orthopyroxene and plagioclase together with troilite in the coarse-grained portion of the object, as well as olivine, pyroxene, and plagioclase from the fine-grained surrounding portion of the object at right.

OVGs). They are usually composed of a fine-grained inner portion and a coarser-grained outer (''overgrowth'') portion (Fig. 9; see also Figs. 1a, 1b, and 4). Table 1 summarizes the petrographic characteristics of the 11 most obvious overgrowth objects, although many other similar objects are present in the meteorite.

The overgrowths of these objects are always dominated by grains of only one silicate mineral, most commonly orthopyroxene, but sometimes olivine, which have one to three crystallographic orientations. Metal, sulfide, and occasionally chromite inclusions are sometimes found enclosed within overgrowth silicates. Some of the metal and sulfide inclusions form crude shell structures concentrated in the inner parts of overgrowths adjacent to the fine-grained interiors (Figs. 9a, 9c, and 9e), whereas others occur in random locations. Little plagioclase is present in the overgrowths, although a few of the objects (OVG 1, 6, 7) are surrounded by plagioclase-rich bands. Overgrowths usually vary in thickness around individual chondrules (Table 1; Figs. 9a and 9f), but in most cases they appear complete and stand out very distinctly from the surrounding host. One object (OVG 8) shows what appears to be a large ''bite'' removed from a portion of the overgrowth, as if it was brecciated following formation (Fig. 9e). In a different object (OVG 1), shock veins crosscut the coarse overgrowth.

The interiors of most OVG objects (OVG 1, 2, 4, 5, 7, 8, 10) are rich in orthopyroxene grains that range in size and texture. All of these pyroxene-rich objects are surrounded by pyroxene overgrowths. The interiors of some objects (OVG 1, 2) contain relatively fine-grained (≤10 μm) equant to elongate pyroxene crystals that tend to be locally aligned, intergrown with small amounts of plagioclase (Fig. 9a). Other objects (OVG 5) have

Table 2. Modal and bulk composition of LITE 3.

	Fine grained facies[1]	Coarse grained facies[2]	Coarse facies, metal-sulfide free	Bulk LITE 3[3]	Average LL chondrite[4]	Average LL chondrite less 70% olivine, metal-sulfide free
Vol%						
Olivine	76.5	11.6		40.4		
Pyroxene[5]	12.6	50.9		33.9		
Plagioclase	10.4	17.1		14.1		
Kamacite	0.1	1.8		1.0		
Taenite	0.4	5.1		3.0		
Troilite		12.3		6.9		
Phosphate		1.3		0.7		
	100.0	100.0		100.0		
Wt%						
SiO_2	41.2	36.6	52.7	38.5	40.58	49.2
TiO_2	< 0.1	0.1	0.2	0.1	0.13	0.2
Al_2O_3	1.8	2.7	3.9	2.3	2.25	3.7
Cr_2O_3	0.1	0.1	0.1	0.1	0.54	0.9
FeO	22.0	9.9	14.3	15.0	17.41	16.4
MnO	0.4	0.3	0.4	0.3	0.34	0.3
MgO	32.2	16.8	24.2	23.3	25.19	23.9
CaO	0.3	1.3	1.8	0.9	1.95	3.2
Na_2O	0.7	1.0	1.4	0.9	0.94	1.6
K_2O	0.1	0.1	0.2	0.1	0.10	0.2
P_2O_5	< 0.1	0.5	0.7	0.3	0.23	0.4
Fe (metal)	0.8	10.7		6.5	2.43	
Ni (metal)	0.3	4.1		2.5	0.98	
Fe (sulfide)	< 0.1	10.0		5.8	3.56	
S	< 0.1	5.8		3.3	2.05	
	100.0	100.0	100.0	100.0	98.68	100.0

[1]Based on point count of BSE image mosaic with 568 total points, assuming kamacite/taenite volume ratio = 0.26/0.74 (= LL chondrite proportion).
[2]Based on point count of BSE image mosaic with 1679 total points, and point count of reflected light images for metal and sulfide assuming kamacite/taenite volume ratio = 0.26/0.74 (= LL chondrite proportion).
[3]Calculated using measured fine/coarse portion ratio = 0.557/0.443.
[4]Jarosewich (1990).
[5]Mostly low Ca pyroxene but includes high Ca pyroxene.

coarser grained (20–30 μm) granular interiors rich in pyroxene, olivine, and plagioclase. Still others (OVG 4, 8) have interiors that are rich in opaque inclusions (mainly troilite and chromite) enclosed within orthopyroxene (Fig. 9e). In the latter objects, interior pyroxene is optically continuous with, and has the same

Fig. 9. (next page) Images of overgrowth objects. a) Transmitted light micrograph of OVG 2 shows a distinct coarse-grained orthopyroxene overgrowth with a concentration of metal and troilite grains (black) on the inner edge of the overgrowth. b) Cross polarized light image of OVG 3. The overgrowth consists of unusually coarse olivine with a single crystallographic orientation. The interior of the object contains a few elongate olivine grains enclosed in mesostasis, forming a texture reminiscent of a barred olivine chondrule. A large chromite grain is intergrown with the olivine shell. c) Backscattered electron micrograph showing a portion of the pyroxene-rich overgrowth and interior of OVG 2. Troilite and metal inclusions are concentrated between the coarser edge and finer-grained interior, although a few larger grains are present within the coarser pyroxene edge. d) Reflected light image of the inner portion of OVG 3 shows mesostasis (mostly plagioclase and micron-sized chromite grains) between coarser olivine grains. e) Cross polarized light micrograph of OVG 8 (outlined), which is chiefly composed of low-Ca pyroxene that is relatively inclusion free at the edge of the object and that contains numerous inclusions in the center of the object. The coarse pyroxene at the object edge has three crystallographic orientations; in this view one of these appears dark at the left side of the object ("*a*"), and the two others appear bright at the right side of the object ("*b*"). A portion of the edge pyroxene appears to be missing at top. f) Transmitted (left and right panels) and cross polarized (center panel) micrographs of OVG 7 show this object in three consecutive thin sections. This object provides a rare example of observing the complex textures of overgrowth objects the way they appear in third dimension. The inner portion of OVG 7 is rich in either fine-grained orthopyroxene (left and center panels) or coarse-grained clinoenstatite (right panel). Clinoenstatite crystals in the right panel appear to radiate from the object edge to fill the entire interior. The olivine overgrowth in the left and center panels mostly has a single crystallographic orientation and some olivine crystals extend inwards toward the object center (most evident in the center panel).

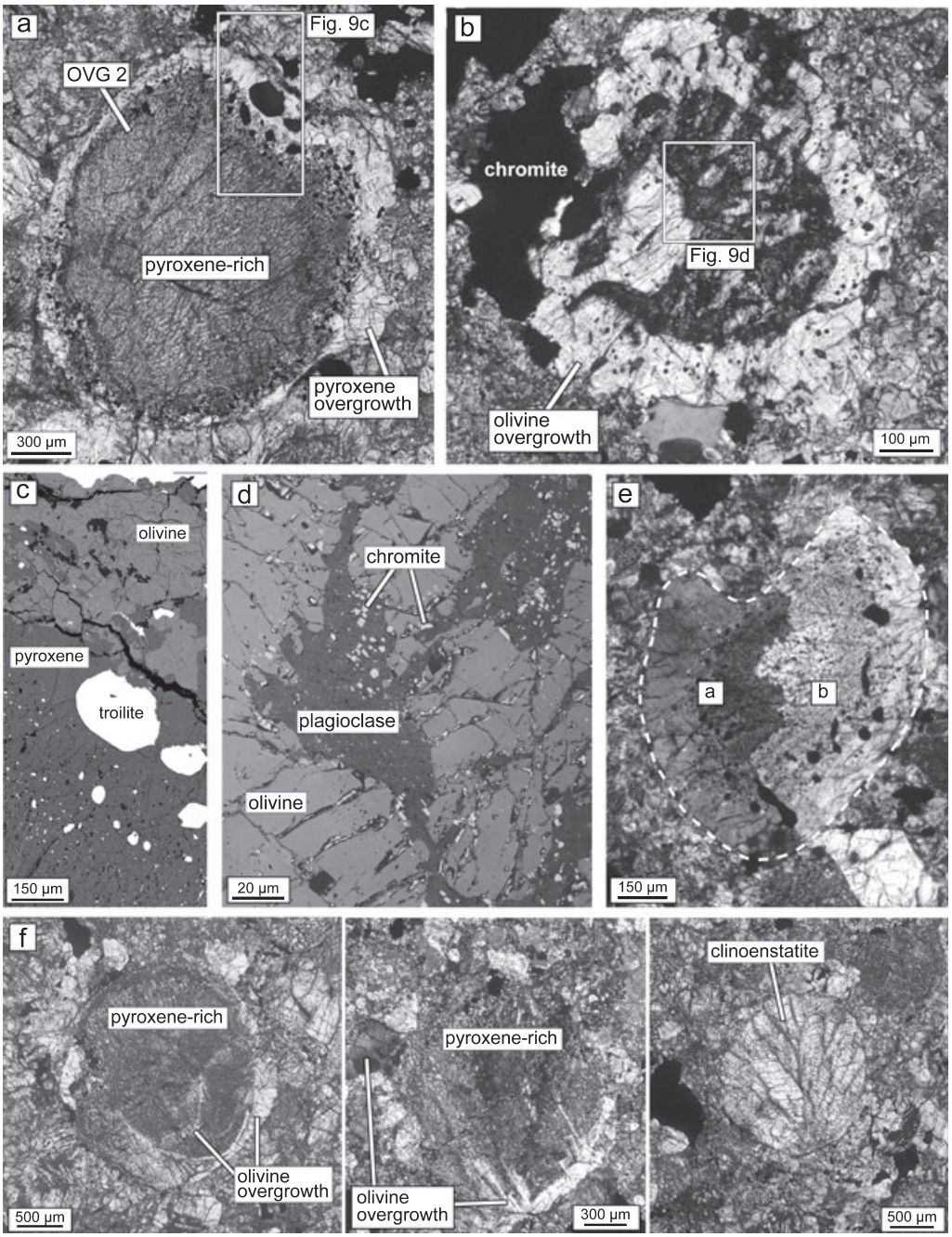

or nearly the same crystallographic orientation as, the adjacent overgrowth pyroxene.

The interiors of two of the objects (OVG 3, 6) contain olivine, plagioclase, and chromite, with the latter two minerals located between elongate to barred olivine grains (Figs. 9b and 9d). Both of these olivine-rich objects are surrounded by olivine overgrowths. Olivine in the overgrowth and the interior of the objects has a single crystallographic orientation.

OVG 7 was sampled in three adjacent thin sections and appears different in these sections (Fig. 9f). In one section, the olivine overgrowth forms laths that extend from the overgrowth toward the center of the fine-grained interior (Fig. 9f, center panel), whereas in another section, the olivine overgrowth appears both at the edge of the object as well as in separate patches with the same crystallographic orientation within the interior (Fig. 9f, left panel). This suggests a complex

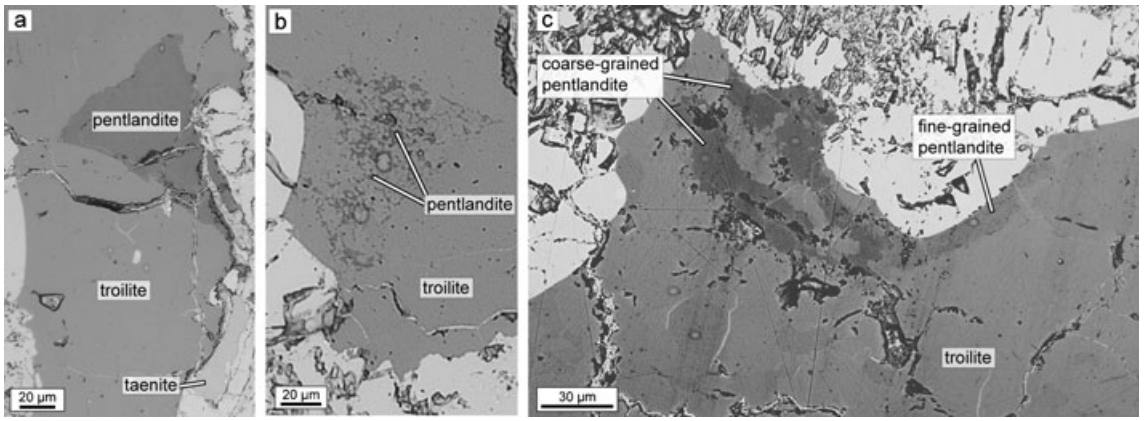

Fig. 10. Pentlandite in reflected light, carbon coated sections. a) Coarse-grained pentlandite that is blocky and has a well-defined boundary. The pentlandite is located inside troilite; a taenite grain is visible in the lower right corner. b) An example of fine-grained pentlandite, present within a troilite grain. The pentlandite forms a lacy texture confined to a restricted portion of the troilite. c) Both coarse and fine pentlandite occur in proximity to one another inside a troilite grain. The coarse pentlandite has a jagged contact against troilite.

three dimensional shape for the coarse olivine. In the third section, the olivine overgrowth is absent and the fine-grained interior is replaced by coarse-grained low-Ca pyroxene (130–200 μm wide) of the clinoenstatite polytype that appears to radiate from a point near the edge of the object (Fig. 9f, right panel).

Occurrence and Textures of Pentlandite

Pentlandite is an accessory mineral in NWA 4859 (present at $<<1$ vol%) but was found in many locations. This mineral has not been extensively studied in meteorites, although it appears to be widely present as a minor constituent in chondrites (Ramdohr 1972; Rubin 2002; this study). It is best observed under reflected light in carbon coated thin sections, and with an approximately 20 nm thick coating, it has strong interference colors of purple-red or brown. In thin sections without a carbon coat, pentlandite is difficult to distinguish from the much more abundant troilite. Small pentlandite grains (<15 μm across) cannot be readily identified without a C-coating.

Pentlandite in NWA 4859 ranges from 2 to about 400 microns across with smaller grains being more abundant. Pentlandite occurs throughout all of the studied thin sections with no preference for location except that it is always found associated with troilite, with pentlandite occurring within and near the edges of troilite grains. Occasionally taenite and/or kamacite grains are found nearby, but mostly pentlandite is not located near metal. Most pentlandite is blocky, with well-defined grain interiors and clearly visible grain boundaries (Fig. 10a). Fine-grained pentlandite has lacy textures with indistinct grain boundaries (Fig. 10b) and is present as small grain patches (5–15 μm across). Blocky and fine-grained pentlandite grains have been observed in close proximity within the same troilite grain (Fig. 10c). Although it is not uncommon to find pentlandite in oxidized (weathered) regions of troilite, pentlandite often occurs in nonoxidized areas, and only a single occurrence of weathered pentlandite was found.

Mineral Compositions

Silicates

The average chemical compositions of silicates in NWA 4859 are shown in Table 3. The compositions of olivine, pyroxene, and plagioclase in the meteorite are consistent with LL ordinary chondrites (Van Schmus and Ribbe 1968; Rubin 1990; Brearley and Jones 1998; Hutchison 2004; Kessel et al. 2007). Olivine ($Fa_{27.8-28.6}$) and low-Ca pyroxene ($En_{74.3–75.8}$, $Fs_{22.7–24.1}$, $Wo_{1.17–2.08}$) grains have relatively uniform compositions throughout the meteorite. This includes grains in the host, LITEs, and OVGs. No zoning in silicates was noted.

Using the two pyroxene geothermometer of Lindsley (1983) and Lindsley and Anderson (1983), low-Ca pyroxene yields an apparent equilibration temperature of 804 ± 24 °C (average and standard deviation based on 35 analyses), and high-Ca pyroxene yields 835 ± 52 °C (based on 4 analyses). Altogether, the pyroxene data suggests pyroxene equilibration at approximately 800–840 °C, which is similar to the temperatures derived for orthopyroxene in LL6 chondrites, and somewhat lower than the temperatures derived for clinopyroxene in LL6 chondrites using the same geothermometer (McSween and Patchen 1989).

Table 3. Chemical composition of silicates of NWA 4859 as determined by electron microprobe analyses.[1]

	Olivine	Orthopyroxene	Clinopyroxene (diopside)	Feldspar
Wt%				
SiO_2	37.5 (0.20)	54.2 (0.46)	52.6 (0.36)	65.1 (0.86)
TiO_2	0.02 (0.02)	0.22 (0.11)	0.39 (0.02)	0.04 (0.02)
Al_2O_3	0.02 (0.03)	0.24 (0.14)	0.48 (0.04)	21.9 (0.44)
Cr_2O_3	0.07 (0.14)	0.14 (0.09)	0.60 (0.06)	0.05 (0.10)
FeO	25.7 (0.21)	15.5 (0.24)	5.44 (0.44)	0.57 (0.35)
MnO	0.45 (0.03)	0.46 (0.03)	0.20 (0.03)	0.02 (0.01)
MgO	36.8 (0.28)	28.1 (0.31)	16.7 (0.40)	0.09 (0.15)
NiO	0.04 (0.04)	0.05 (0.03)	0.13 (0.06)	0.06 (0.06)
CaO	0.02 (0.01)	0.83 (0.13)	22.1 (0.42)	2.58 (0.40)
Na_2O	0.02 (0.01)	0.03 (0.04)	0.39 (0.06)	8.26 (0.31)
K_2O	n.d.	n.d.	n.d.	0.97 (0.25)
Total	100.6	99.8	99.1	99.7
Mol%				
Fa	28.2 (0.18)			
En		75.1 (0.34)	46.9 (0.91)	
Fs		23.3 (0.28)	8.6 (0.68)	
Wo		1.59 (0.25)	44.6 (0.88)	
Ab				80.0 (2.1)
An				13.8 (2.1)
Or				6.2 (1.6)
N	37	37	4	32

[1]Mean compositions, with standard deviations indicated in parentheses, *N*, number of analyses; n.d., not detected.

Table 4. Chemical composition of metal and sulfide phases as determined by electron microprobe analyses.[1]

	Troilite	Kamacite	Taenite	Tetrataenite	Pentlandite[2]	Pentlandite[3]
Fe	63.3 (0.4)	91.5 (1.1)	63.6 (1.1)	46.4 (1.1)	48.4 (2.3)	47.7 (0.6)
Ni	0.04 (0.03)	5.46 (0.4)	34.8[4] (1.1)	52.9 (0.7)	16.4 (1.3)	17.1 (0.6)
S	36.5 (0.3)	0.01 (0.01)	0.01 (0.01)	0.03 (0)	33.1 (1.2)	33.5 (0.2)
Co	0.01 (0.01)	2.67 (0.3)	1.46 (0.07)	0.56 (0.3)	1.27 (0.48)	0.77 (0.12)
Cr	0.02 (0.03)	n.d.	0.02 (0.03)	0.03 (0.04)	0.01 (−)	0.01 (−)
Total	99.9	99.6	99.8	100.0	99.2	99.1
N	63	12	32	2	12	15
#Gr	32	5	16	2	5	13

[1]Mean compositions in wt%, with standard deviations indicated in parentheses. N, number of analyses; #Gr, number of analyzed grains; n.d., not detected.
[2]Fine-grained pentlandite.
[3]Coarse-grained pentlandite.
[4]Two Ni-rich analyses not included in this table would have raised Ni content to 35.2 (2.3).

Metals and Sulfides

Chemical analyses of metals and sulfides are reported in Table 4. The average compositions of metal phases in NWA 4859 are consistent with the average composition in LL chondrites (Afiattalab and Wasson 1980; Rubin 1990, 2002; Brearley and Jones 1998). The composition of pentlandite, troilite, and metal in NWA 4859 is shown in a Fe-Ni-S ternary diagram in Fig. 11, and the Ni-Co composition of pentlandite and metal is shown in Fig. 12.

The overall average Ni content of pentlandite (approximately 16.8 wt%, Table 4) appears to be deficient when compared with pentlandite stability fields at temperatures of 230–850 °C (Shewman and Clark 1970; Craig 1973; Sukagi and Kitakaze 1998; Raghavan 2004; Bullock et al. 2005) (Fig. 11). Analyses of pentlandite grains show that coarse and fine grains vary in Co content (Fig. 12). The cobalt content of fine-grained pentlandite (12 analyses of 5 different grains) has a wide range compared with the closely clustered coarse grains (15 analyses of 13 grains). Although compositions overlap, fine-grained pentlandite grains have more variable and a slightly lower average Ni content than coarse-grained pentlandite grains (Fig. 12;

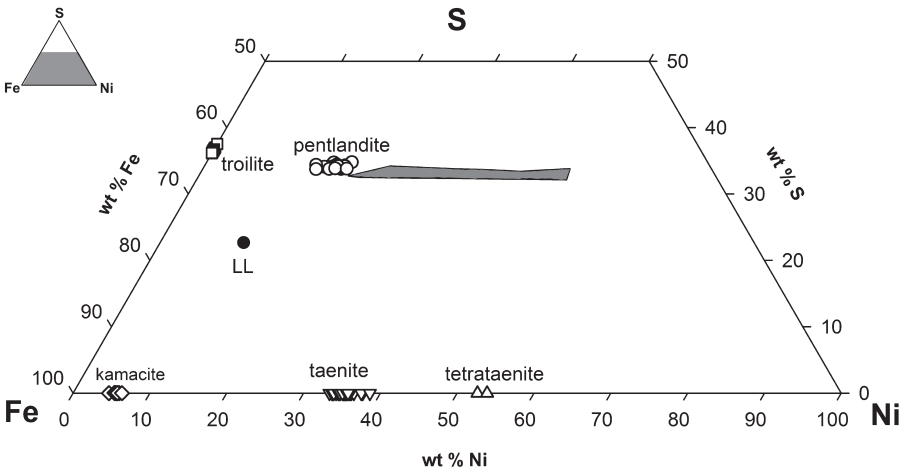

Fig. 11. Fe-Ni-S ternary diagram showing composition of metal and sulfide phases in NWA 4859, and the pentlandite stability field at temperatures between 230 and 850 °C (Shewman and Clark 1970; Misra and Fleet 1973; Sukagi and Kitakaze 1998; Sinyakova and Kosyakov 2001; Etschmann et al. 2004; Raghavan 2004; Fleet 2006). "LL" is the bulk metal and sulfide composition of 18 LL chondrites of type 3–6 (Jarosewich 1990). Tie lines drawn between troilite and taenite, or between troilite and tetrataenite, divide pentlandite from the bulk LL point, implying that pentlandite should not coexist stably with troilite, kamacite, and either taenite or tetrataenite in a system of bulk LL composition.

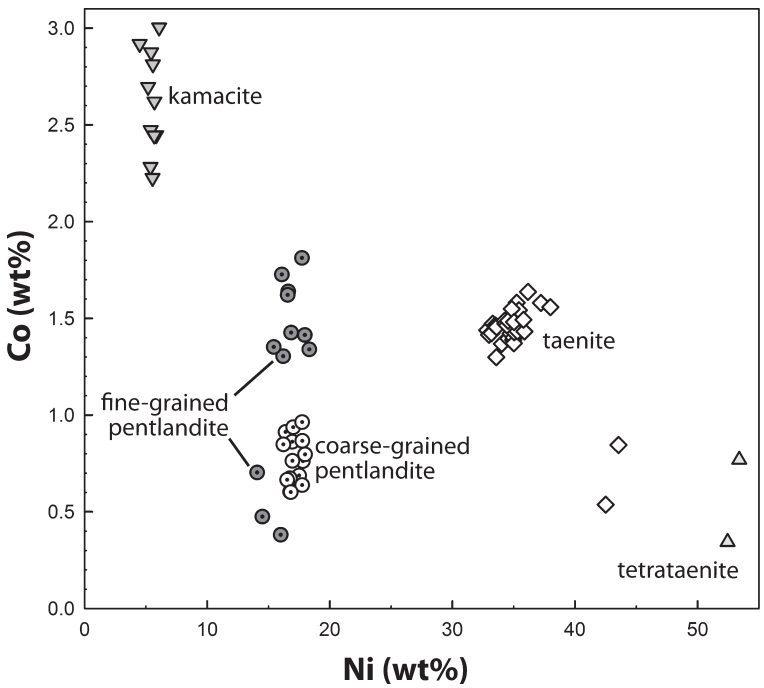

Fig. 12. Co versus Ni diagram shows composition fields of metals and sulfides in NWA 4859. Fine-grained pentlandite has more variable Co content than coarse-grained pentlandite.

Table 4). We also found zoning in three of the coarse-grained pentlandite grains. From grain cores to rims, this change in chemical composition involves approximately 0.3 wt% decrease in S, approximately 0.5–2.0 wt% increase in Fe, and approximately 0.7–1.8 wt% decrease in Ni.

Pentlandite compositions in NWA 4859 differ from those reported in other meteorites (Lauretta et al. 2001; Bullock et al. 2005; Engrand et al. 2007), but most closely resemble several grains in Ustï nad Orlici (L6), where Bukovanská et al. (1983) reported a "secondary sulfide" (pentlandite) composition that closely matches

our sample. However, unlike NWA 4859, Bukovanská et al. also reported significantly different compositions among different pentlandite grains in the same meteorite, differing in Ni and Fe by as much as 9 wt% each.

DISCUSSION

Parentage and Petrographic Type

We infer an LL protolith for NWA 4859 based on the overall textures, mineralogy, and mineral compositions of the meteorite. NWA 4859 shows areas with chondritic texture, and the meteorite contains silicate proportions similar to an ordinary chondrite, i.e., it is rich in olivine and low-Ca pyroxene and contains less plagioclase feldspar. The abundance of metal and sulfides is consistent with the LL group. Also consistent with this group are the phase compositions measured in NWA 4859. The Fa content in olivine and Fs content in pyroxenes (Table 3), the cobalt and nickel content in kamacite (Fig. 12; Table 4), and the An/Ab/Or content in plagioclase (Table 3) are all consistent with LL chondrite (Brearley and Jones 1998).

It is not obvious whether a type 5 or type 6 designation is more appropriate for the LL protolith. In some areas, chondrules appear to be readily recognizable as for type 5, whereas in other areas, they are barely recognizable as for type 6. The situation is complicated by the presence of distinct appearing OVG objects that may not be chondrules, which may not be appropriate to use as markers of textural integration. The range of Wo content in low-Ca pyroxene suggests a type 6 designation (Scott et al. 1986; Brearley and Jones 1998). In addition, two pyroxene thermometry performed according to Lindsley (1983) and Lindsley and Anderson (1983) implies that the closure temperature for orthopyroxene in NWA 4859 is similar to that in type 6 chondrites. We do not claim, however, that the temperatures obtained with two pyroxene thermometry represent the maximum temperature recorded in the meteorite. It is possible that the meteorite was heated to higher temperatures and cooled slowly afterward, reaching a closure temperature for diffusion in orthopyroxene similar to that in type 6 chondrites. If the meteorite cooled slowly, it would explain why orthopyroxene and clinopyroxene in NWA 4859 yield similar closure temperatures, somewhat unlike what is typically found for type 6 chondrites (McSween and Patchen 1989). We suggest that the chondritic host of NWA 4859 was initially a type 5 chondrite that experienced additional shock-related heating and melting, thereby resulting in some type 6-like characteristics. To acknowledge this ambiguity, we refer to the host chondrite as type 5–6, but even so it should be recognized that this host is atypical for a chondrite in that it contains plagioclase-rich bands.

Origin of LITEs

Large, igneous-textured enclaves clearly were once substantially molten. Here, we discuss their possible origins.

The textures found in most LITEs in NWA 4859 (i.e., barred olivine, porphyritic olivine) are similar to large chondrule-like melt objects, i.e., macrochondrules or megachondrules (Binns 1967; Bridges and Hutchison 1997; Ruzicka et al. 1998). Thus, one possibility is that LITEs are simply unusually large chondrules. However, some LITEs have textures dissimilar to normal chondrules. For example, so far as we are aware, the "donuts" present in LITE 4 have never been described as features within chondrules, although they do bear some resemblance to whole barred olivine chondrules. Also, the dichotomous object LITE 3 and the coarse granular object LITE 2 have textures that are atypical for chondrules. Furthermore, although it is not too uncommon to find an occasional megachondrule in a chondrite, it seems unlikely that NWA 4859 would have sampled so many of these objects compared with other chondrites. This is particularly true as unambiguous chondrules in the meteorite are not especially large, implying that large objects were not preferentially accumulated in NWA 4859. Thus, it seems unlikely that the LITEs are simply megachondrules.

Alternatively, the LITEs in NWA 4859 could have originated as clasts from an external igneous source (Hutchison et al. 1988; Kennedy et al. 1992; Bridges and Hutchison 1997; Ruzicka et al. 1998). With this model, the different textures observed in enclaves would require that multiple types of igneous rocks were sampled by NWA 4859. However, it seems unlikely that NWA 4859 sampled clasts from so many varied external sources compared with other ordinary chondrites. It is also not clear if LITEs are clasts, as they typically lack well-defined edges. Although indistinct margins could be explained by postagglomeration metamorphism, coarse-grained interior borders in LITEs are unlikely to be produced by metamorphism. Instead, these coarse interior borders are more consistent with crystallization processes that could have occurred in the LITEs adjacent to original (unbroken) margins.

LITEs also could have originated as shock melts that were injected into the host meteorite. If this was the case, one would expect to see chill margins produced by the contact of a melt and a cold host, which could be represented by glassy or fine-grained

edges. Such chill zones have been reported in a large olivine microporphyry of inferred shock melt origin in the St. Mesmin chondrite (Dodd and Jarosewich 1976) but were not observed in any of the enclaves in NWA 4859. Indeed, far from having chill margins, the LITEs in NWA 4859 often have the opposite—comparatively coarse-grained, well-crystallized borders.

An intrusive (injection) shock melt origin would be consistent with the observations if the temperature of the host were elevated at the time of the intrusions. This would be possible if the surrounding host was heated by the simultaneous emplacement of multiple LITE melts at the time of melt injection, or if the host was deeply buried and undergoing thermal metamorphism at the time of melt injection. In either case, it appears as if LITE emplacement was followed by slow cooling, which would explain the lack of chill margins or glass, the blurred boundaries of the LITEs, and the equilibrated composition of silicates in the enclaves and the surrounding host. One can explain "interior borders" as the result of physical interactions between partly solidified shock melt and surrounding host, with coarse crystals accumulating along the edge of the melt area adjacent to the host. We conclude that an intrusive shock melt origin for the LITEs is likely.

Although a shock melt origin for LITEs with emplacement into warm host is consistent with the observations, certain mechanisms are required to create textural variations of LITEs. We speculate that all of the enclaves originated from melts generated during a single shock event and that different LITE textures can be explained by differences in the original temperatures of the melts and their subsequent cooling histories. Differences in maximum temperatures could arise by deriving LITE melts from slightly different source areas heated to differing extent in a large impact event, whereas differences in effective cooling histories can arise by bringing variably heated melts to the same (relatively high) ambient temperature. Arguing by analogy to chondrule studies (e.g., Gooding and Keil 1981; Lofgren and Russell 1986; Lofgren 1989, 1996; Hewins and Radomsky 1990; Hewins and Connolly 1996; Hewins 1997; Connolly et al. 1998), we suggest that barred and skeletal olivine-rich LITEs were derived from an almost complete melt where all but a few of the pre-existing olivine grain nuclei were destroyed. We suggest that differences in grain sizes for barred and skeletal LITEs are related to the degree of undercooling they experienced, with finer-grained barred/skeletal objects (e.g., LITE 5 and the olivine-rich portion of LITE 3) cooling more quickly at higher temperatures than coarser-grained barred objects (e.g., LITE 9). Porphyritic olivine enclaves could have originated from a less strongly heated but more slowly cooling melt, for which more nuclei were preserved at maximum temperature and the extent of undercooling was less. The large size of phenocrysts in porphyritic olivine LITEs compared with normal sized microporphyritic olivine chondrules could indicate that melts in LITEs were either more extensively heated or less undercooled than chondrules.

"Donuts" in LITE 4 could have formed by crystallization from separate, single crystal nuclei, in a fashion similar to barred olivine chondrules. Besides having a barred morphology, donuts often have overall sizes that resemble chondrules. It is possible that donuts were derived from pre-existing olivine rich chondrules that were partly melted. Rare donuts found in the host could represent objects separated from LITE melts during the emplacement of the LITEs into the host.

Our model thus suggests that different LITE textures arose chiefly as a result of having different numbers of nuclei present in melts. Except possibly for the donuts in LITE 4, there is no obvious evidence for clastic debris within the LITEs, so the LITEs themselves are not "shock-melt clasts" in the usual sense of the term (e.g., as given by Bischoff et al. 2005). Moreover, as discussed previously, the LITEs are probably not "clasts," in that they are not simply rock fragments. Thus, it is inappropriate to refer to the LITEs either as "shock-melt clasts" or "clasts." Rather, they represent "shock melts" (bodies that were substantially molten) injected into a chondritic host.

The composition, mineralogy, and dichotomous texture of LITE 3 implies a complex origin. We infer that LITE 3 formed by shock melting of LL chondrite, that it experienced a two-stage cooling history together with significant phase separation during fractional crystallization, and that it represents a rare example of a differentiated object in a chondrite. Skeletal olivine from the fine-grained outer portion could have crystallized as a liquidus phase during the transit of hot source melt into the cooler, final emplacement location within NWA 4859. This would result in initial rapid cooling of the olivine and would explain its fine-grained, skeletal textures. After crystallization of skeletal olivine, the liquid remaining in an adjacent area could have crystallized to form pyroxene, plagioclase, metal, troilite, and phosphate in what would become the coarse-grained portion of the object. Coarser and more equigranular grains of these phases in the coarse facies of LITE 3 imply cooling at a slow rate, with melt being insulated by the surrounding host and the already crystallized olivine. Besides textures, this scenario is strongly supported by the overall composition of LITE 3, which is similar to LL chondrite, and by the composition of the coarse portion, which is similar to what one would obtain by the removal of olivine from LL chondrite.

An alternative interpretation of the coarse portion of the LITE is that it represents a clast that was enveloped by shock melt that solidified to form the fine-grained portion of the LITE. However, this interpretation cannot explain the overall chondritic composition of LITE 3 as anything but coincidence, whereas the chondritic composition makes sense if the entire object was produced by shock melting of chondrite. Moreover, whereas the overall object has chondritic composition, the two components of LITE 3 are chemically distinctive and complementary, with the fine-grained portion unusually rich and the coarser-grained portion unusually poor in olivine. For these two chemically distinctive materials to occur intergrown without being genetically related seems unlikely. Furthermore, as the fine-grained portion of the LITE is much more olivine-rich than the coarse portion, it would have had a higher melting temperature, so there would be a tendency for the high-temperature melt to assimilate the low temperature material if the latter was a clast. But the contact between the two portions is relatively sharp, and there is no evidence for assimilation. Finally, the texture and mineralogy of the coarse portion of LITE 3 is distinctive and atypical for the meteorite (including twinned plagioclase, which was observed only in LITE 3), so it does not seem likely that it would be randomly found as a clast inside a shock melt. Instead, the two facies of LITE 3 are probably genetically related and crystallized from the same, differentiating parent melt.

As far as we are aware, differentiation of the type implied for LITE 3 has not previously been reported for a chondrite. However, this occurrence may not be unique in NWA 4859 as smaller areas with textures and mineralogies similar to the coarse and fine portions of LITE 3 are rarely observed elsewhere in the meteorite.

Olivine is a predominant phase in most LITEs as well as in LL chondrites. This suggests that most LITEs could have formed by shock melting of average LL chondrite. However, LITE 2 alone is pyroxene-rich. This object could have been derived by melting of a pyroxene-rich area of an LL chondrite source. This would require either melting of a large pyroxene-rich chondrule or accumulation of pyroxene during melting or crystallization. Alternatively, LITE 2 was derived from a chondritic melt that underwent significant fractionation. If the latter, the melt would have had to lose both a high temperature olivine-rich and low temperature feldspathic component, requiring a complex petrogenesis.

Most LITEs (except for LITE 3) are poor in metal and sulfide. Thus, if these objects formed by melting of whole rock chondrite, metal and sulfide must have been segregated. These phases would tend to form an immiscible liquid that could have separated from the silicate melts during the emplacement of these melts into the host. It is possible that the coarse sulfides found in NWA 4859 represent this separated immiscible melt. The high concentration of troilite and metal in LITE 3 implies that metallic liquids were not able to separate from this LITE, so LITE emplacement did not always result in the loss of such metallic liquid.

Origin of Plagioclase-rich Bands

Plagioclase bands are not found in chondritic meteorites that were affected by thermal metamorphism, so they do not belong to regular metamorphic series of ordinary chondrites. We infer that they originated as a melt surrounding chondrules, LITEs, and other objects. Crystallization from such a melt is consistent with the polymineralic nature of the bands, which are composed of mafic minerals in addition to plagioclase feldspar, and with the euhedral–subhedral textures of the mafic minerals. It is unlikely that the melt was generated by a slow and gradual heating event, as this would lead to a somewhat uniform igneous texture in the surrounding rock, not the mixture of chondritic texture and plagioclase-rich bands that is actually found in NWA 4859.

By contrast, a short duration and high intensity heating event of a chondrite protolith, such as one during collisional shock, would result in temperatures reaching above the solidus for a short duration of time, potentially melting areas interstitial to coarser grains and chondrules while still retaining an overall chondritic texture of the rock. Circular plagioclase-rich areas, some of which are chromite rich, probably originated in the same way, by crystallization from a melt.

A shock melt origin for the plagioclase bands and other plagioclase-rich regions is supported by previous work on similar features found in other chondrites. This includes interstitial feldspar-rich regions in ordinary chondrite regolith breccias (Bischoff et al. 1983; Bischoff and Stöffler 1992), feldspathic areas in the annealed Spade chondrite (Rubin and Jones 2003), and plagioclase–chromite assemblages in many chondrites (Rubin 2003). The bands in NWA 4859 texturally resemble the interstitial feldspathic regions in regolith breccias (Bischoff and Stöffler 1992; Bischoff et al. 1983; see especially fig. 22 of the latter), except that in NWA 4859, there is less evidence for the incorporation of obvious mafic mineral clasts, and more evidence that olivine and pyroxene could have crystallized from melt. We suggest that this difference reflects a greater degree of melting in NWA 4859, caused either by more intense shock metamorphism or by shock occurring at elevated

temperatures, or both. According to Bischoff and Stöffler (1992), interstitial plagioclase in the most intensely shocked (Class C) ordinary chondrite regolith breccias formed at shock pressures >15–30 GPa, implying this as a lower limit for the formation of plagioclase bands in NWA 4859. The cutoff between S3 and S4, and between S4 and S5, is approximately 15–20 and 30–35 GPa, respectively (Stöffler et al. 1991), so a shock stage of roughly ≥S4 is implied by the plagioclase bands. Although this shock stage for the bands in NWA 4859 is uncertain, an S4 shock stage agrees with the level of deformation observed for olivine in the host, suggesting that both this deformation and the formation of plagioclase bands could have been generated by the same shock event.

The plagioclase bands lack the fine-grained metal and troilite droplets found in typical pseudotachylite veins produced by shock melting. This implies that metal and sulfide did not quench together with silicates in the plagioclase bands. The bands are present around most large objects in the NWA 4859, but are absent around coarse sulfide grains. We suggest that the bands formed by relatively slow crystallization, which enabled all silicate melt to crystallize and immiscible metal and sulfide liquids to accumulate into larger masses that became separated from the silicate melts. Thus, silicate melts crystallized as plagioclase bands, and S-rich melts crystallized as unusually coarse troilite grains. Similarly, we suggest that coarse phosphate grains in NWA 4859 could have crystallized from localized pockets of P-rich melt that may have immiscibly separated from both silicate and sulfide liquids.

Origin of OVG Objects

Textural observations of the OVG objects imply that the overgrowth portions could have grown from melts with only a few (1–3) crystal nuclei. This contrasts with the fine-grained interiors of the objects, which probably crystallized from multiple nuclei. Most likely OVG objects were partly molten in their interiors and almost completely molten in their outer portions. The textures of the objects can be explained by radially directed crystallization of olivine or pyroxene in the overgrowth portion. Inward directed growth is suggested by the texture of olivine in one section of OVG 7, which shows projections that taper inwards from the coarse outer border (center panel of Fig. 9f). It is possible that OVG objects formed by partial re-melting of chondrules or chondrule-like objects during the high temperature shock melting event that also produced LITEs and plagioclase-rich bands. Such a chondrule-derived origin for OVGs is supported by the sizes of OVG objects, which are similar to chondrules, and the observation that the mineralogy of OVG objects is dominated by either olivine or pyroxene as is common for chondrules. It is unclear whether these objects formed in situ in the host, or whether they were injected into the host while partly molten. In any case, the occurrence of plagioclase bands composed of a low-melting-temperature assemblage that sometimes surround OVG objects implies that the outer shell of OVG objects crystallized before the bands.

Origin of Pentlandite

Unlike LITEs, OVG objects, and plagioclase-rich bands in NWA 4859, the authors have observed pentlandite with similar textures and in similar settings (i.e., with pentlandite occurring in troilite as blocky or lacy forms) in other ordinary chondrites. This suggests that the formation of this mineral does not require special circumstances. Despite previous statements to the contrary (Ramdohr 1973), it is not unusual to find pentlandite in meteorites with free iron. However, it is true that pentlandite is rarely, if ever, found in direct contact with metal alloy.

We suggest that pentlandite in NWA 4859 mostly formed out of equilibrium and that its presence records local processes. Evidence for this includes the following. (1) Based on the Gibbs phase rule, pentlandite cannot coexist in equilibrium with troilite, kamacite, taenite, tetrataenite, and vapor, as this would require a variance of −1, which is thermodynamically impossible. These minerals are all present in NWA 4859, and S-bearing vapor was likely present at the time of formation, implying that disequilibrium was important. (2) The topology of the Fe–Ni–S phase diagram (e.g., Craig and Scott 1976) implies that for a system of bulk LL composition, an equilibrium phase assemblage would be troilite + kamacite + taenite (or troilite + kamacite + tetrataenite depending on temperature). Thus, pentlandite either did not form in equilibrium, or did not form in a system of bulk LL composition, or both. (3) The composition of pentlandite in NWA 4859 approaches but does not overlap reported equilibrium compositions for pentlandite produced with a large variety of bulk compositions and temperatures (230–850 °C) (Fig. 11). Thus, pentlandite in NWA 4859 probably did not form in equilibrium over this temperature range.

In principle, pentlandite in NWA 4859 could form by sulfidation of metal (reaction of metal with S-bearing vapors) (Lauretta et al. 1997a,b), but we do not consider this likely as there is no textural evidence for replacement of metal by sulfide in NWA 4859. Another possibility is that pentlandite could form by oxidation of Fe metal, which would drive the local bulk composition into a sufficiently Fe-poor, Ni-rich and S-rich condition to

stabilize pentlandite. However, this process would be expected to result in unusually Fe-poor, Ni-rich metal, for which there is no evidence in NWA 4859.

As pentlandite is always located within troilite, another possibility is that the pentlandite and troilite formed together by reaction with another phase. At high temperatures, the monosulfide solid solution (*mss*) phase is the most prevalent sulfide (Craig and Scott 1976), which can react at lower temperatures to form pentlandite and other sulfide minerals such as pyrrhotite or troilite (Hawley and Haw 1957; Kullerud 1963; Naldrett et al. 1967; Misra and Fleet 1973; Francis et al. 1976; Durazzo and Taylor 1982; Kelly and Vaughan 1983). *Mss* has a wide solid solution range and can accommodate large amounts of Ni, but the formation of Ni-poor troilite will leave excess Ni behind that must be accommodated by another phase. In complete equilibrium, one might expect Ni to diffuse out of the *mss* precursor and diffuse into coexisting metal at the time of troilite formation, but if diffusion was limited at low temperatures, this might not be possible, and pentlandite would form inside the troilite instead. Some of the pentlandite in NWA 4859 is zoned, which is consistent with the idea of limited diffusion. In support of our model, Lauretta et al. (1997b) found that diffusion-limited effects and local equilibrium were likely important for troilite at typical metamorphic temperatures in ordinary chondrites. As pentlandite and troilite could have formed together, this inference for troilite is relevant for pentlandite as well.

Formation of pentlandite and troilite by the breakdown of *mss* monosulfide is consistent with the different textures observed for pentlandite in NWA 4859. Different textures of pentlandite can be produced by breakdown of *mss* depending on diffusion rates and the initial degree of supersaturation, with more "blocky" pentlandite forming at higher temperatures and more irregular "flames" forming at lower temperatures (e.g., Durazzo and Taylor 1982). In NWA 4859, we suggest that the coarse, blocky pentlandite represents a relatively large degree of grain growth and that it formed at higher temperatures; and that the fine-grained, lacy pentlandite represents less grain growth and a lower formation temperature. This model is consistent with the larger spread of Co and Ni contents in the fine, lacy pentlandite compared with the coarse pentlandite (Fig. 12), which can be explained by less equilibration in fine-grained pentlandite caused by more sluggish diffusion at lower temperatures. The slightly lower average Ni content for lacy pentlandite is also consistent with a lower formation temperature, for the reasons given below.

The composition of pentlandite depends both on temperature and bulk composition. For example, Shewman and Clark (1970) found that the Ni/Fe ratio in pentlandite decreases as equilibrium temperature drops. However, at the lowest temperature investigated by these researchers (400 °C), Ni/Fe in pentlandite is still higher than in NWA 4859. Similarly, Misra and Fleet (1973) found that pentlandite has the lowest Ni contents when it coexists with troilite, in what are relatively Ni-poor systems. Pentlandite in NWA 4859 has a Ni/Fe value that most closely resembles, and which is only slightly less than, pentlandite coexisting with troilite at a temperature of 230 °C (Misra and Fleet 1973).

Considering the effects of temperature and bulk composition, pentlandite in NWA 4859 probably formed at low temperature (≤230 °C) in a Ni-poor sulfide (*mss*) system. Judging from the low temperature phase diagram for Fe–Ni (Yang et al. 1996), a similarly low closure temperature (≤250 °C) is implied by the presence of Ni-rich (approximately 53 wt% Ni) tetrataenite in NWA 4859. Thus, for NWA 4859, cooling rates at such low temperatures evidently were sufficiently slow to allow both pentlandite and tetrataenite to form locally.

Shock and Thermal History of NWA 4859

Based on petrographic and mineral–chemical studies, we conclude that NWA 4859 experienced at least two collisional events. These events were of different intensity and occurred under different conditions.

An early and high intensity shock event could have been responsible for the formation of LITEs, OVGs, and plagioclase-rich bands. LITEs were injected as melts into a chondritic host, whereas OVGs could have been partly molten chondrules that were either also transported before final emplacement or were peripherally melted in situ. During this early heating event, plagioclase, troilite, and phosphate in the host were partly melted, with plagioclase crystallizing in bands and troilite and phosphate crystallizing in large grains. An extended period of annealing followed the shock, implying that shock and melt emplacement occurred at depth within the parent body, probably below a large impact crater, possibly while the target was being heated during thermal metamorphism.

A second, less intense, shock event that affected NWA 4859 was responsible for the formation of opaque shock veins that crosscut the host, LITEs, OVGs, and plagioclase bands, and which displaced some of the coarse troilite grains. This late shock can be characterized as an S3 shock stage event, which is consistent with presence of the veins, with the minimum shock stage observed for olivine in LITEs, and with the absence of maskelynite. This shock event probably was responsible for producing twinned pyroxene with the clinoenstatite structure occasionally found throughout

the meteorite. The preservation of the clinoenstatite implies limited postshock annealing, so the second shock event must have involved little heating. Limited annealing in the second event is consistent with the variable shock stages shown by olivine grains in different LITEs and the host, which otherwise might have been annealed to the same, low shock stage. On the other hand, the lack of glass in the opaque veins implies that they did not cool rapidly, so evidently the meteorite was not brought close to a cooling surface by the second shock event, and cooling occurred at depth within the parent body. There is no evidence that the second shock occurred while the host was warm, so it probably took place well after thermal metamorphism.

The less deformed olivine grains in LITEs compared with the host is explained by deriving LITEs from largely molten shock-melt and the injection of these melts into the host that experienced a lower degree of melting, and which consequently preserved more evidence for shock deformation up to that point. Thus, the shock stage of the host (S4) is somewhat higher than the late shock event (S3) as it records both the late deformation as well as the earlier deformation associated with melt emplacement.

The presence of pentlandite also places constraints on the thermal history experienced by NWA 4859. The occurrence of this mineral and its Ni-poor composition suggests that it formed at low temperature (mainly < 230 °C), in response to slow cooling. The postshock temperature increase estimated for an S3 shock stage event is approximately 50–200 °C (Stöffler et al. 1991). Although this amount of heating was probably too mild to have caused much inversion of clinoenstatite to orthoenstatite, it could have been important for transformations in sulfides. Thus, pentlandite could have formed in response to heating in the second shock event. *Mss* is stable over a range of compositions at temperatures as low as approximately 100–300 °C (Craig and Scott 1976), so the second shock event could have created *mss* if it was not already present, which then decomposed to pentlandite + troilite upon cooling.

Classification of NWA 4859

The classification of NWA 4859 is not straightforward owing to the complicated history that the meteorite experienced. The rock is clearly an impact-melt breccia, in that parts were shock melted, and parts were not. All of the unusual features in the meteorite, including LITEs, OVG objects, plagioclase-rich bands, and coarse grains of troilite, can be explained as having formed by the crystallization of shock-induced melts. LITE melts formed elsewhere and were transported into the host, where they crystallized while partially molten. As these melts were substantially molten, they were probably formed under $>$S6 shock stage conditions. They were injected into a LL host chondrite that was probably of petrographic type 5, but which may have been locally heated by the injection of shock melt to the equivalent of petrographic type 6. The host was partly melted to form plagioclase bands under conditions equivalent to shock stage ≥S4, and deformed to produce plastic deformation in coarse olivine grains equivalent to shock stage S4. The shock-melt breccia was then annealed by relatively slow cooling. A distinctly later shock event of S3 shock stage was overprinted on the breccia, which resulted in mild heating, and in the formation of opaque veins, pyroxene of the clinoenstatite polytype, and pentlandite. Thus, by combining all available evidence, NWA 4859 can be accurately described as an annealed impact-melt breccia with LL5-6 (S4) host that experienced early, localized shock melting and a late S3 shock stage event.

CONCLUSION

NWA 4859 is a meteorite of LL chondrite parentage that experienced a complex shock and thermal history. The meteorite contains unusual features, which include a high proportion of large (up to 3 cm across) igneous-textured enclaves (LITEs) of various textures (commonly olivine microporphyry or barred/skeletal), chondrule-sized objects with coarse-grained borders composed of a small number of either low-Ca pyroxene or olivine crystals (OVG objects), plagioclase-rich bands that encircle most other objects, and unusually coarse sulfide grains (up to 7 mm). The meteorite also contains a minor proportion ($<<1\%$) of pentlandite intergrown with troilite, which, although not generally recognized, does not appear to be unusual for an ordinary chondrite. We suggest that all of the unusual features of the meteorite can be explained by the crystallization of shock-induced melts followed by slow cooling at depth within the parent body. LITE shock melts evidently were intruded into an LL protolith, with one such melt region undergoing differentiation following emplacement. Plagioclase-rich bands, coarse troilite, and OVG objects all appear to have formed by the crystallization of localized melts. Shock heating may have occurred contemporaneously with thermal metamorphism. Following this early heating, NWA 4859 was shocked again to an S3 level, but the extent of annealing following shock was much less in this case. Pentlandite and troilite formed by the breakdown of a monosulfide precursor phase at low (≤230 °C) temperatures, during slow cooling following the second shock. The occurrence of pentlandite in ordinary chondrites may reflect common, mild heating events. NWA 4859 is an annealed

impact-melt breccia with an LL5-6 host that experienced at least two shock events.

Acknowledgments—The authors would like to thank Edwin Thompson for his generous donation of NWA 4859 sample, Melinda Hutson for her help in classifying NWA 4859, Addi Bischoff, Dante Lauretta, and Adrian Brearley for helpful reviews, and the supporters of the Cascadia Meteorite Laboratory for their donations and funding that made this research possible.

Editorial Handling—Dr. Adrian Brearley

REFERENCES

Afiattalab F. and Wasson J. T. 1980. Composition of the metal phases in ordinary chondrites: Implications regarding classification and metamorphism. *Geochimica et Cosmochimica Acta* 44:431–446.

Bennett M. E. and McSween H. Y. 1996. Revised model calculations for the thermal histories of ordinary chondrite parent bodies. *Meteoritics & Planetary Science* 31:783–792.

Binns R. A. 1967. An exceptionally large chondrule in Parnallee meteorite. *Mineralogical Magazine* 36:319–324.

Bischoff A. and Stöffler D. 1992. Shock metamorphism as a fundamental process in the evolution of planetary bodies: Information from meteorites. *European Journal of Mineralogy* 4:707–755.

Bischoff A., Rubin A. E., Keil K., and Stöffler D. 1983. Lithification of gas-rich chondrite regolith breccias by grain boundary and localized shock melting. *Earth and Planetary Science Letters* 66:1–10.

Bischoff A., Scott E. R. D., Metzler K., and Goodrich C. A. 2005. Nature and origins of meteoritic breccias. In *Meteorites and early solar system II*, edited by Lauretta D. S., Harry J., and McSween Y. Tucson, AZ: The University of Arizona Press. pp. 679–712.

Brearley A. J. and Jones R. H. 1998. Chondritic meteorites. In *Planetary materials*, edited by Papike J. J. Washington, D.C.: Mineralogical Society of America. pp. 3.1–3.398.

Bridges J. C. and Hutchison R. 1997. A survey of clasts and large chondrules in ordinary chondrites. *Meteoritics & Planetary Science* 32:389–394.

Bukovanská M., Jakeš P., Pernicka E., and El Goresy A. 1983. Ustï nad orlici: A new L6 chondrite from czechoslovakia. *Meteoritics* 18:223–239.

Bullock E. S., Gounelle M., Lauretta D. S., Grady M. M., and Russell S. S. 2005. Mineralogy and texture of Fe–Ni sulfides in CI1 chondrites: Clues to the extent of aqueous alteration on the CI1 parent body. *Geochimica et Cosmochimica Acta* 69:2687–2700.

Connolly H. C., Jr., Jones B. D., and Hewins R. H. 1998. The flash melting of chondrules: An experimental investigation into the melting history and physical nature of chondrule precursors. *Geochimica et Cosmochimica Acta* 62:2725–2735.

Craig J. R. 1973. Pyrite-pentlandite assemblages and other low temperature relations in the Fe-Ni-S system. *American Journal of Science* 273A:496–510.

Craig J. R. and Scott S. D. 1976. Sulfide phase equilibria. In *Sulfide mineralogy*, edited by Ribbe P. H. Washington, D.C.: Mineralogical Society of America. pp. CS1–CS110.

Dodd R. T. and Jarosewich E. 1976. Olivine microporphyry in the St. Mesmin chondrite. *Meteoritics* 11:1–20.

Durazzo A. and Taylor L. A. 1982. Exsolution in the mss-pentlandite system: Textural and genetic implications for ni-sulfide ores. *Mineralium Deposita* 17:313–332.

Engrand C., Duprat J., Maurette M., and Gounelle M. 2007. Fe–Ni sulfides in concordia Antarctic micrometeorites (abstract #1668). 38th Lunar and Planetary Science Conference. CD-ROM.

Etschmann B., Pring A., Putnis A., Grguric B. A., and Studer A. 2004. A kinetic study of the exsolution of pentlandite (Ni, Fe)9S8 from the monosulfide solid solution (Fe, Ni)S. *American Mineralogist* 89:39–50.

Fleet M. E. 2006. Phase equilibria at high temperatures. In Reviews in mineralogy and geochemistry, edited by Russo J. J. Chantilly, VA: The Mineralogical Society of America. pp. 365–419.

Francis C. A., Fleet M. E., Misra K. C., and Craig J. R. 1976. Orientation of exsolved pentlandite in natural and synthetic nickeliferous pyrrhotite. *Americal Mineralogist* 61:913–920.

Gaines R. V., Skinner H. C. W., Foord E. E., Mason B., and Rosenzweig A. 1997. *Dana's new mineralogy: The system of mineralogy of James Dwight Dana and Edward Salisbury Dana*. New York: John Wiley & Sons, Inc.

Gooding J. L. and Keil K. 1981. Relative abundances of chondrule primary textural types in ordinary chondrites and their bearing on conditions of chondrule formation. *Meteoritics* 16:17–43.

Hawley J. E. and Haw V. A. 1957. Intergrowths of pentlandite and pyrrhotite. *Economic Geology* 52:132–139.

Hewins R. H. 1997. Chondrules. *Annual Review of Earth and Planetary Sciences* 25:61–83.

Hewins R. H. and Connolly H. C., Jr. 1996. Peak temperatures of flash-melted chondrules. In *Chondrules and the protoplanetary disk*, edited by Hewins R. H., Jones R. H., and Scott E. R. D. Cambridge, UK: Cambridge University Press. pp. 197–204.

Hewins R. H. and Radomsky P. M. 1990. Temperature conditions for chondrule formation. *Meteoritics* 25:309–318.

Hutchison R. 2004. *Meteorites: A petrologic, chemical and isotopic synthesis*. Cambridge, UK: Cambridge University Press. 506 p.

Hutchison R., Williams C. T., Din V. K., Clayton R. N., Kirschbaum C., Paul R. L., and Lipschutz M. E. 1988. A planetary, H-group pebble in the Barwell L6, unshocked chondrite meteorite. *Earth and Planetary Science Letters* 90:105–118.

Jarosewich E. 1990. Chemical analysis of meteorites: A compilation of and stony and iron meteorite analyses. *Meteoritics* 25:323–327.

Kelly D. P. and Vaughan D. J. 1983. Pyrrhotite-pentlandite ore textures: A mechanistic approach. *Mineralogical Magazine* 47:453–463.

Kennedy A. K., Hutchison R., Hutcheon I. D., and Agrell S. O. 1992. A unique high Mn/Fe microgabbro in Parnallee (LL3) ordinary chondrite: Nebular mixture or planetary differentiate from a previously unrecognized planetary body? *Earth and Planetary Science Letters* 113:191–205.

Kessel R., Beckett J., and Stolper E. 2007. The thermal history of equilibrated ordinary chondrites and relationship between textural maturity and temperature. *Geochimica et Cosmochimica Acta* 71:1855–1881.

Kullerud G. 1963. Thermal stability of pentlandite. *The Canadian Mineralogist* 7:353–366.

Lauretta D. S., Lodders K., and Fegley B. J. 1997a. Experimental simulations of sulfide formation in the solar nebula. *Science* 277:358–360.

Lauretta D. S., Lodders K., and Fegley B. J. 1997b. The origin of sulfide-rimmed metal grains in ordinary chondrites. *Earth and Planetary Science Letters* 151:289–301.

Lauretta D. T., Buseck P. R., and Zega T. J. 2001. Opaque minerals in matrix of the Bishunpur (LL3.1) chondrite: Constraints on the chondrule formation environment. *Geochimica et Cosmochimica Acta* 65:1337–1353.

Lindsley D. H. 1983. Pyroxene thermometry. *American Mineralogist* 68:477–493.

Lindsley D. H. and Anderson D. J. 1983. A two-pyroxene thermometer. *Journal of Geophysical Research* 88:A887–A906.

Lofgren G. 1989. Dynamic crystallization of chondrule melts of porphyritic olivine composition: Textural experimants and nature. *Geochimica et Cosmochimica Acta* 53:461–470.

Lofgren G. 1996. A dynamic crystallization model for chondrule melts. In *Chondrules and the protoplanetary disk*, edited by Hewins R. H., Jones R. H., and Scott E. R. D. Cambridge, UK: Cambridge University Press. pp. 187–196.

Lofgren G. and Russell W. J. 1986. Dymanic crystallization of chondrule melts of pyrphyritic and radial pyroxene composition. *Geochimica et Cosmochimica Acta* 50:1715–1726.

McSween H. Y. and Patchen A. D. 1989. Pyroxene thermobarometry in LL-group chondrites and implications for parent body metamorphism. *Meteoritics* 24:219–226.

Misra K. C. and Fleet M. E. 1973. The chemical compositions of synthetic and natural pentlandite assemblages. *Economic Geology* 68:518–539.

Nagahara H. 1983. Chondrules formed through incomplete melting of the pre-existing mineral clusters and the origin of chondrules. In *Chondrules and their origins*, edited by King E. A. Huston, TX: Lunar and Planetary Institute. pp. 211–222.

Naldrett A. J., Craig J. R., and Kullerud G. 1967. The central portion of the Fe-Ni-S system and its bearing on pentlandite exsolution in iron–nickel sulfide ores. *Economic Geology* 62:826–847.

Raghavan V. 2004. Fe-Ni-S (Iron-Nickel-Sulfur). *Journal of phase equilibria and diffusion* 25:373–381.

Ramdohr P. 1972. Lunar pentlandite and sulfiidization reaction in microbreccia 14315, 9. *Earth and Planetary Science Letters* 15:113–115.

Ramdohr P. 1973. *The opaque minerals in stony meteorites*. New York, NY: Elesevier Publishing Company.

Reed S. J. B. and Chinner G. A. 1995. The Bawku LL5 chondrite. *Meteoritics* 30:468–469.

Rubin A. E. 1990. Kamacite and olivine in ordinary chondrites: Intergroup and intragroup relationships. *Geochimica et Cosmochimica Acta* 54:1217–1232.

Rubin A. E. 2002. Post shock annealing of Miller Range 99301 (LL6) : Implications for impact heating of ordinary chondrites. *Geochimica et Cosmochimica Acta* 66:3327–3337.

Rubin A. E. 2003. Chromite–plagioclase assemblages as a new shock indicator; implications for the shock and thermal histories of ordinary chondrites. *Geochimica et Cosmochimica Acta* 67:2695–2709.

Rubin A. E. and Jones R. H. 2003. Spade: An H chondrite impact-melt breccia that experienced post-shock annealing. *Meteoritics & Planetary Science* 38:1507–1520.

Ruzicka A., Snyder G., and Taylor L. A. 1998. Mega-chondrules and large, igneous-textured clasts in Julesberg (L3) an dother ordinary chondrites: Vapor-fractionation, shock-melting, and chondrule formation. *Geochimica et Cosmochimica Acta* 62:1419–1442.

Ruzicka A., Snyder G., and Taylor L. A. 2000. Geochemical and isotopic evidence bearing on the origin of large, igneous-textured inclusions in ordinary chondrites. *Antarctic Meteorite Research* 13:19–38.

Schmitt R. T. 2000. Shock experiments with the H6 chondrite Kernouvé: Pressure calibration of microscopic shock effects. *Meteoritics & Planetary Science* 35:545–560.

Schmitt R. T. and Stöffler D. 1995. Experimental data in support of the 1991 shock classification of chondrites. *Meteoritics* 30:574–575.

Scott E. R. D., McKinley S. G., Keil K., and Wilson I. E. 1986. Recovery and classification of thirty new meteorites from Roosevelt County, New Mexico. *Meteoritics* 21:303–308.

Sharp T. G. and DeCarli P. S. 2006. Shock effects in meteorites. In *Meteorites and early solar system II*, edited by Lauretta D. S., Harry J., and McSween Y. Tucson, AZ: The University of Arizona Press. pp. 653–677.

Shewman R. W. and Clark L. A. 1970. Pentlandite phase relations in the Fe-Ni-S system and notes on the monosulfide solid solution. *Canadian Journal of Earth Sciences* 7:67–86.

Sinyakova E. F. and Kosyakov V. I. 2001. 600 C section of the Fe-Ni-S-NiS-Ni phase diagram. *Inorganic Materials* 37:1130–1137.

Stöffler D., Keil K., and Scott E. R. D. 1991. Shock metamorphism or ordinary chindrites. *Geochimica et Cosmochimica Acta* 55:3845–3867.

Sukagi A. and Kitakaze A. 1998. High form of pentlandite and its thermal stability. *American Mineralogist* 83:133–140.

Van Schmus W. R. and Ribbe P. H. 1968. The composition and structural state of feldspar from chondritic meteorites. *Geochimica et Cosmochimica Acta* 32:1327–1342.

Wlotzka F. 1993. A weathering scale for ordinary chondrites. *Meteoritics* 28:460.

Yang C.-W., Williams D. B., and Goldstein J. I. 1996. A revision of the Fe-No phase diagram at low temperatures ($< 400^{o}$ C). *Journal of Phase Equilibria* 17:522–531.